

1  
2  
3  
4  
5 **Volcanically-Induced Transient Atmospheres on the Moon:**  
6 **Assessment of Duration, Significance and Contributions to Polar Volatile**  
7 **Traps**  
8  
9  
10

11 **James W. Head<sup>1</sup>, Lionel Wilson<sup>1,2</sup>, Ariel N. Deutsch<sup>1</sup>, Malcolm J. Rutherford<sup>1</sup>, and**  
12 **Alberto E. Saal<sup>1</sup>**

13 <sup>1</sup>Department of Earth, Environmental and Planetary Sciences, Brown University,  
14 Providence, RI 02912 USA.

15 <sup>2</sup>Lancaster Environment Centre, Lancaster University, Lancaster LA1 4YQ UK.

16  
17 Corresponding author: James Head ([james\\_head@brown.edu](mailto:james_head@brown.edu))  
18

19 **Key Points:**

- 20 • A transient lunar atmosphere from peak volcanic degassing lasting up to ~70 Ma  
21 was recently proposed as a source of lunar polar volatiles.
- 22 • We forward-model individual eruption volume, degassing patterns, and duration  
23 of periods between eruptions (repose periods), finding that:
- 24 • Transient, volcanically-induced atmospheres are inefficient sources for volatile  
25 delivery to permanently shadowed lunar polar regions.  
26

## 27 **Abstract**

28 A transient lunar atmosphere formed during a peak period of volcanic outgassing and  
29 lasting up to about ~70 Ma was recently proposed. We utilize forward-modeling of  
30 individual lunar basaltic eruptions and the observed geologic record to predict eruption  
31 frequency, magma volumes, and rates of volcanic volatile release. Typical lunar mare  
32 basalt eruptions have volumes of  $\sim 10^2$ - $10^3$  km<sup>3</sup>, last less than a year, and have a rapidly  
33 decreasing volatile release rate. The total volume of lunar mare basalts erupted is small  
34 and the repose period between individual eruptions is predicted to range from 20,000-  
35 60,000 years. Only under very exceptional circumstances could sufficient volatiles be  
36 released in a single eruption to create a transient atmosphere with a pressure as large as  
37 ~0.5 Pa. The frequency of eruptions was likely too low to sustain any such atmosphere  
38 for more than a few thousand years. Transient, volcanically-induced atmospheres were  
39 probably inefficient sources for volatile delivery to permanently shadowed lunar polar  
40 regions.

41

## 42 **Plain Language Summary**

43 Could gas emitted from volcanic eruptions during the most intense and voluminous  
44 period of lunar mare volcanism produce a temporary lunar atmosphere? Could the  
45 presence of such an atmosphere enable volatiles to reach the cold traps in the  
46 permanently shadowed regions at the lunar poles? We use information from lunar  
47 geology and sample analyses to predict the number of eruptions with time, the volume of  
48 individual eruptions, the rates of volcanic gas release during each eruption, and the time  
49 between eruptions. We find that only under rare circumstances could a single eruption or  
50 two eruptions closely-spaced in time release enough gas to create a transient atmosphere  
51 with a pressure as large as ~0.5 Pa. Furthermore, it is difficult to sustain such an  
52 atmosphere for more than a few thousand years. These results suggest that volcanically-  
53 produced atmospheres are inefficient source mechanisms for delivery of volatiles to form  
54 deposits in permanently shadowed polar regions of the Moon; this favors volatile-rich  
55 impactors as the major source of polar ice.

56

## 57 **1 Introduction**

58 The current atmosphere of the Moon is a stable, low-density surface boundary  
59 exosphere ( $\sim 10^{-12}$  mbar) (Stern, 1999; Cook et al., 2013; Benna et al., 2015) and is  
60 thought to have changed little in the last several billion years. Volcanism, a significant  
61 source of volatile supply to planetary atmospheres throughout planetary history, is known  
62 to have been much more important in early lunar history (mare basalt volcanism; Shearer  
63 et al., 2008; Head and Wilson, 2017), spanning from over 4 billion years ago (beginning  
64 with cryptomaria; Whitten et al., 2015a,b), reaching peak fluxes between 3 and 4 Ga, and  
65 declining to much lower levels between 3 and 1 Ga (Hiesinger et al., 2011; Pasckert et  
66 al., 2015; Head et al., 2020).

67 Needham and Kring (2017) assessed lunar mare basalt volcanic flux estimates and  
68 volatile release abundances to address whether these patterns might lead to a transient or  
69 sustained lunar atmosphere early in lunar history. Using the distribution and quantity of  
70 mare basalt fill, and estimates of its age, they calculated the magma flux (the volume of  
71 mare basalt erupted as a function of time), and then estimated the corresponding release

72 rate of volatiles on the basis of estimates derived from the analysis of lunar samples (e.g.,  
 73 Saal et al., 2008; Rutherford and Papale, 2009; Hauri et al., 2011; Kring, 2014). Using  
 74 estimates of mare basalt unit ages (e.g., Hiesinger et al., 2011) and thicknesses (Weider et  
 75 al., 2010), Needham and Kring (2017) concluded that during a period of peak mare  
 76 emplacement and volcanic volatile release at ~3.5 Ga (Figs. S1a,b), the maximum  
 77 atmospheric pressure at the lunar surface could have reached ~1 kPa (~1.5 times greater  
 78 than the current atmospheric surface pressure of Mars) (Fig. S1c) and that this lunar  
 79 atmosphere could have persisted for ~70 million years before fully dissipating (Fig. S1c).  
 80 They further pointed out that even though most of the volcanically-released volatiles will  
 81 have been lost to space, if only 0.1% of the water released during these eruptions  
 82 migrated to the permanently shadowed polar regions of the Moon, then the resulting  
 83 hydrogen mass could account for the entire currently observed hydrogen deposits located  
 84 there (Eke et al., 2009; Livengood et al., 2018).

85 We adopt a different approach, using improved models of the generation, ascent  
 86 and eruption of lunar basaltic magma (Wilson and Head, 2017), to predict flow volumes,  
 87 eruption frequencies (Head and Wilson, 2017), and temporal magmatic volatile release  
 88 patterns in individual eruptions (Rutherford et al., 2017; Wilson and Head, 2018). Key  
 89 components of this analysis are 1) the range (and mean value) of magma volumes erupted  
 90 in individual eruptions, 2) the masses, and hence volumes, of the various gases released  
 91 in any one eruption, 3) the duration of the eruption and the gas release rate (varying  
 92 significantly as the eruption progresses), 4) the typical time intervals between eruptions  
 93 (repose periods) as a function of geologic time and 5) the timescale for the dissipation of  
 94 an atmosphere once one is emplaced. We review the geological basis for the first four  
 95 components, examine the potential time-dependence and variability of gas release in an  
 96 individual typical eruption, and finally address the question: *Are these gas-release values*  
 97 *sufficient to form a transient atmosphere and, if so, for what duration?* We then compare  
 98 our findings with the broad-scale, time-averaged peak flux estimates of Needham and  
 99 Kring (2017) (see the Supporting Material), and address similarities and differences and  
 100 their causes, and how estimates might be refined in the future. We conclude by assessing  
 101 whether the forward-modeling predictions of gas-release rates are sufficient to: 1) act as a  
 102 significant supply of volatiles to the permanently shadowed lunar polar cold-trap regions  
 103 and 2) form a transient lunar atmosphere for a period sufficient to favor astrobiological  
 104 activity as suggested by Schulze-Makuch and Crawford (2018).  
 105

## 106 **2 Forward Modeling Lunar Mare Basaltic Eruptions**

107 Wilson and Head (2017) and Head and Wilson (2017) improved earlier  
 108 theoretical models for the generation, ascent and eruption of basaltic magma on the Moon  
 109 (Wilson and Head, 1981; Head and Wilson, 1992) by using new data on crustal thickness  
 110 and density (Wieczorek et al., 2013), magma volatile inventories (Rutherford et al.,  
 111 2017), and surface morphology, topography and structure (from Lunar Reconnaissance  
 112 Orbiter). They showed that ongoing partial melting in buoyant diapirs deep in the mantle  
 113 overpressurizes the source regions, producing sufficient stress to cause brittle fracturing;  
 114 a magma-filled crack grows, disconnects from its source and propagates to the surface as  
 115 a blade-shaped, convex-upward dike. The typical turbulent magma rise speeds that result  
 116 are ~10 to a few tens of  $\text{m s}^{-1}$ , dike widths are ~100 m, and eruption rates from 1-10 km  
 117 long fissure vents are  $\sim 10^5$  to  $10^6 \text{ m}^3 \text{ s}^{-1}$ . Lunar eruption volume fluxes derived from lava

118 sinuous rille lengths and depths or flow thicknesses and surface slopes are  $\sim 10^5$  to  $10^6$  m<sup>3</sup>  
 119 s<sup>-1</sup> (volume-limited lava flows) and  $>10^4$  to  $10^5$  m<sup>3</sup> s<sup>-1</sup> (rilles). The volume of magma  
 120 released in one event is predicted to be in the range  $10^2$ - $10^3$  km<sup>3</sup> (Wilson and Head, 2017;  
 121 Head and Wilson, 2017). Thus, if all the magma were extruded from these dike events  
 122 and spread evenly across the surface in 25 m thick flows, they would occupy areas of  
 123 4000 to 40,000 km<sup>2</sup>, well within the range of thicknesses and areas of mapped and dated  
 124 (e.g., Hiesinger et al., 2011) lunar mare lava flows. We now summarize aspects of these  
 125 treatments to derive the relevant parameters.

126 2.1) Individual mare basalt eruption volumes: Range and typical values:  
 127 Individual eruption volumes of typical visible, and therefore most recent, lava flow  
 128 deposits, are at least  $\sim 200$ - $300$  km<sup>3</sup> (Head and Wilson, 2017) (Table 1a). In addition,  
 129 Head and Wilson (1981) estimated the minimum volume of lava,  $\sim 100$  km<sup>3</sup>, needed to  
 130 thermo-mechanically erode the preserved sinuous rille channels. Applying the same  
 131 method to the largest lunar rille, Schroeter's Valley, implies a volume of  $2000$  km<sup>3</sup> and a  
 132 duration of  $\sim 150$  days. On the basis of these predictions and observations, we adopt a  
 133 range of individual eruption volumes,  $V$ , of  $100$ - $2000$  km<sup>3</sup> (Table 1a), with typical values  
 134 in the range  $100$ - $300$  km<sup>3</sup>.

135 2.2) Total mare basalt erupted volumes: Using mare basin lava fill depth  
 136 estimates, the total volume,  $V_t$ , of all volcanic products erupted on the Moon over its  
 137 lifetime is  $\sim 10^7$  km<sup>3</sup> (Head and Wilson, 1992; Evans et al., 2016). The absolute dates of  
 138 specific eruptions are unknown, but crater size-frequency distribution-derived dates of  
 139 units mapped from orbit, and stratigraphic relationships, imply that the overall time span  
 140 of the vast majority of lunar volcanic activity was  $\sim 2$  Ga (Hiesinger et al., 2011; Head  
 141 and Wilson, 2017; Head et al., 2020).

142 2.3) Number of eruptions, average eruption rates, and estimated repose periods:  
 143 Using the  $100$ - $300$  km<sup>3</sup> average eruption volume, the  $\sim 10^7$  km<sup>3</sup> total erupted volume of  
 144 mare basalts, and the  $\sim 2$  Ga duration of volcanism, we calculate a total of  $\sim 30,000$  to  
 145  $100,000$  eruptions with an average repose period of  $20,000$  to  $60,000$  years. These repose  
 146 times assume that eruptions occur randomly in space and time, in which case two  
 147 eruptions might occur with a much smaller time interval; however, we show in the  
 148 Supplementary Material that eruptions at intervals close enough in time to influence our  
 149 conclusions will be rare. Accounting for lunar thermal evolution (conductive cooling and  
 150 lithospheric thickening) in terms of mare mantle production rates and the evolving  
 151 lithospheric stress state and magnitude (Head and Wilson, 2017), we would predict  
 152 decreasing volumes of magma with time. If three times as much magma was erupted in  
 153 the  $4$ - $3$  Ga period than in the  $3$ - $2$  Ga period, for example, the earlier eruptions would have  
 154 occurred every  $13,000$  to  $40,000$  years.

155 2.4) Eruption durations: Analyses of the dynamics of lunar eruptions allow us to  
 156 estimate the volume fluxes,  $F_1$ , of lava forming surface flows and sinuous rilles (Wilson  
 157 and Head 2017; Head and Wilson, 2017); coupled with the typical erupted volumes  
 158 described above, these give values for the typical durations,  $\tau_e$ , of these eruptions (Table  
 159 1a), all less than  $6$  months, with most eruption durations in the  $1$ - $3$  month range.

160 2.5) Magmatic volatiles and volatile release patterns: Analyses of lavas and  
 161 pyroclastics sampled by the Apollo missions (Saal et al., 2008; Rutherford and Papale,  
 162 2009; Hauri et al., 2011; Chen et al., 2015; Rutherford et al., 2017; Renggli et al., 2017;  
 163 Ni et al., 2019) provide estimates for the compositions and amounts of released volatiles.

164 The highest amount is that for picritic magmas, ~3400 ppm (Rutherford et al., 2017). At  
 165 the other extreme, Head and Wilson (2017) found that the radii of the lava ponds feeding  
 166 the lava flows eroding sinuous rille channels imply total magma volatile contents of no  
 167 more than 700 ppm. We adopt 2000 ppm, close to the average of these extremes. The  
 168 Rutherford et al. (2017) volatiles are CO, H<sub>2</sub>O, SO<sub>2</sub>, H<sub>2</sub>S, COS and F present in amounts  
 169  $n_i$  of 1395, 1133, 327, 168, 327 and 50 ppm, respectively, and with molecular masses  $m_i$   
 170 of 28.0, 18.0, 64.1, 34.1, 60.1 and 19.0, respectively, the mean molecular weight is  $\Sigma (n_i$   
 171  $m_i) / \Sigma n_i = 31.4 \text{ kg kmol}^{-1}$ . The corresponding values for alternative compositions  
 172 suggested by Renggli et al. (2017) and Newcombe et al. (2017) are 48.9 and 22.2 kg  
 173  $\text{kmol}^{-1}$ , respectively; we adopt the Rutherford et al. (2017) value as typical for subsequent  
 174 calculations.

175 2.6) Volatile input to the atmosphere: We first calculate the *total volume of gas*  
 176 *released* from an eruption of a specific volume, and then analyze the *time-history of gas*  
 177 *release in the several phases of an individual eruption* (Rutherford et al., 2017; Wilson  
 178 and Head, 2018). Multiplying the dense-rock-equivalent erupted volume  $V$  by the typical  
 179 density of lunar basaltic magma,  $\rho_m = \sim 3000 \text{ kg m}^{-3}$ , yields the magma mass erupted, and  
 180 multiplying that by the total released gas mass fraction  $n_t = \Sigma n_i$  gives the total gas mass  
 181 released,  $M_g$ . Finally dividing  $M_g$  by  $\tau_e$  yields the average gas mass input rate to the  
 182 atmosphere,  $F_g$ . Table 1a summarizes these values. However, gas release during an  
 183 eruption is non-linear, and typically declines with time (Wallace et al., 2015). Speciation,  
 184 relative abundances and fluxes of specific volatiles can vary during a single eruption.  
 185 Could such variations in individual volcanic eruptions result in spikes in volatile output  
 186 contributing to an atmosphere that might be underestimated by deriving an average value  
 187 for the entire eruption? We now employ an updated version of a recent model of the  
 188 typical phases of a lunar eruption to assess these questions.

189 Wilson and Head (2018), using data from Rutherford et al. (2017), assessed mare  
 190 basalt gas release patterns during individual volcanic eruptions as a basis for predicting  
 191 the effect of sequential gas production, bubble nucleation and growth, magma and gas  
 192 rise rates, bubble coalescence, and magma disruption processes. Subdividing typical  
 193 lunar eruptions into four phases (Fig. 1a), they showed how these phases of mare basalt  
 194 eruption, together with total dike volumes, initial magma volatile content, vent  
 195 configuration, and magma discharge rate, could assist in relating the wide range of  
 196 seemingly disparate volcanic features to a common set of eruption processes. Figure 1  
 197 updates the values given by Wilson and Head (2018) using a more detailed integration of  
 198 the eruption rate model based on work in progress.

199 In Phase 1, which is very short-lived, the rising dike penetrates to the surface, and  
 200 initiates *the transient gas release phase*. This very explosive phase is due to  
 201 concentration of volatiles into a low-pressure area near the upper propagating dike tip  
 202 (Wilson & Head, 2003). Pure gas may extend 100–200 m down from the top of the dike,  
 203 above a high vesicularity foam layer extending downward ~10 km. Eruption of this gas-  
 204 rich magma dike tip takes as little as a few minutes, resulting in an extremely thin but  
 205 very widespread deposit, consistent with volcanic glass beads ubiquitous in lunar soils.

206 During Phase 2, *the high-flux hawaiian eruptive phase*, the dike continues to rise  
 207 toward a neutral buoyancy configuration. This phase is characterized by the highest  
 208 magma discharge rate during the eruption,  $\sim 10^6 \text{ m}^3/\text{s}$ , involving a near-steady explosive  
 209 magma eruption; the volatile content is representative of the bulk of the magma. This

210 phase is characterized by formation of a relatively steady hawaiian fire fountain, largely  
 211 optically dense. Submillimeter-sized pyroclastic droplets lose gas efficiently and  
 212 accumulate with negligible cooling within a few to 10 km of the fissure, forming a lava  
 213 lake deficient in gas bubbles. For a short-lived eruption, lava that is largely degassed  
 214 flows away from the lake, initially turbulently, to form the distal part of the final lava  
 215 flow deposit. For a sufficiently long-lasting eruption, the lava will feed a flow eroding a  
 216 sinuous rille. More than 80% of the total dike magma volume would have been erupted  
 217 during this phase; the erupted magma volume flux decreases from  $\sim 10^6$  to  $\sim 10^5 \text{ m}^3 \text{ s}^{-1}$   
 218 over its typical 2-3 day duration.

219 Phase 3, the lower flux *hawaiian to strombolian transition phase* begins when the  
 220 positive buoyancy of the lower part of the dike in the mantle balances the negative  
 221 buoyancy of the upper part in the crust, and the eruption-feeding dike approaches an  
 222 equilibrium. The lower dike tip stops rising, and fixing the vertical extent of the dike. The  
 223 main driving process in this phase becomes the horizontal reduction in dike thickness due  
 224 to: 1) decrease in internal excess pressure, and 2) relaxation of forced host rock  
 225 deformation due to initial dike intrusion (Wilson & Head, 2017). Shallow crust host rock  
 226 deformation is probably elastic and rapid; hotter mantle rock deformation (surrounding  
 227 the lower part of the dike) is more likely to be visco-elastic or viscous; this results in a  
 228 much longer closure timescale. Magma vertical rise speed in the dike decreases greatly  
 229 (to less than 1 m/s) during this period; this implies that the magma volume flux leaving  
 230 the vent decreases similarly to a few  $\times 10^4 \text{ m}^3 \text{ s}^{-1}$  during  $\sim 3$ -5 days. Reduction in vertical  
 231 magma flow speed means that nucleating gas bubbles throughout the dike vertical extent  
 232 can now rise through the liquid at an appreciable rate. There is ample time for larger  
 233 bubbles to overtake smaller bubbles (especially CO bubbles being produced at great  
 234 depths). This leads to coalescence and even greater growth; this in turn leads to very  
 235 large bubbles—gas slugs—filling almost all of the dike width and producing strombolian  
 236 surface explosions (Parfitt & Wilson, 1995). The transition from hawaiian activity (Phase  
 237 2) to strombolian (Phase 3) occurs rapidly.

238 Phase 4, the *dike closing, strombolian vesicular flow phase*, begins when the  
 239 activity becomes entirely strombolian. Horizontal dike closure continues due to tectonic  
 240 stresses and magma is extruded at a low flux. Magma from the deepest dike parts  
 241 continues to be forced upward to lower pressure levels thus continuing to produce some  
 242 CO at all depths; the result is very minor, but continuing strombolian explosive activity  
 243 above the vent. For magma still emerging from the vent, a stable crust will form and flow  
 244 away as lava.

245 Two different pathways might occur during Phase 4 activity. In *low flux eruptions*  
 246 (Phase 4a), Phase 4 might begin following of eruption of most of the magma in the dike  
 247 and the volume flux has decreased to a very low level (Fig. 1a). Wilson and Head (2017)  
 248 predict that the result will be the emplacement of vesicular lava in the vicinity of the vent  
 249 as a series of cooling-limited flows potentially building a small, low shield. Erupted  
 250 magma consists of liquid which contains bubbles (a mixture of gases and volatile  
 251 elements) (Gaillard & Scaillet, 2014; Renggli et al., 2017; Saal et al., 2018). These are  
 252 determined by the thermodynamic equilibrium between the products of interactions  
 253 (mainly between  $\text{H}_2\text{O}$  and sulfur species) released over the last  $<500$  m of magma flux.  
 254 Such gas bubbles would nucleate with diameters of  $\sim 10$ – $20 \mu\text{m}$  and grow to  $\sim 20$ – $30 \mu\text{m}$   
 255 at the surface; they remain stable within the lava (surface tension forces impose a

256 retaining pressure of ~30 kPa; Wilson & Head, 2017). Lavas exsolving ~1,000 ppm of  
257 such gases would leave the vent as lava foams with vesicularities >90% by volume. The  
258 topmost bubbles would likely have exploded into the overlying vacuum; this should  
259 produce a layer of bubble wall shards, and gas escapes easily through this accumulating  
260 debris layer until welding of particles and accumulated debris weight inhibited further  
261 foam disintegration. If the underlying lava still contained dissolved volatiles, the  
262 unvesiculated layer could become important during further lava cooling and  
263 crystallization if volatile concentration into the remaining liquid resulted in second  
264 boiling and additional post-emplacement vesiculation. Volatile contributions to the  
265 atmosphere of these latter-stage processes would be minimal, however, as the rates of  
266 diffusive volatile loss from vesiculated cooling and cooled lavas are extremely low.

267 A second potential outcome is predicted to occur in dikes that are vertically more  
268 extensive (Phase 4b, high flux). If a large fraction of total dike magma remains available  
269 for extrusion as vesicular lava, this lava can readily intrude into the still-hot interiors of  
270 the previously emplaced nonvesicular flows and cause flow inflation. The shallow parts  
271 (<400 m depth) of a dike feeding such intruding/inflating flows would contain not yet  
272 exsolved water and sulfur compounds. The resulting inflated flows would cool on a  
273 timescale of weeks: volatile concentration into the residual liquid as crystallization  
274 occurred would then lead to second boiling. The new population of gas bubbles could  
275 cause a possibly extensive further inflation episode (Wilson et al., 2019). The resulting  
276 magmatic foam and gas could escape through cracks in the lava crust caused by inflation,  
277 but again the gas flux into the atmosphere would be minimal.

278 Eruption Phase 4 duration is controlled by the global stress state of the lithosphere  
279 (both its nature and magnitude), influencing host rocks visco-elastic relaxation, and by  
280 magma cooling in the dike. Lunar thermal history (Solomon & Head, 1980) suggests  
281 extensional lithospheric stresses during the first ~1 Ga, followed by compressive stresses  
282 at ~3.6 Ga as the interior cooled. This would encourage more closure of dikes in  
283 geologically more recent eruptions. Dike models (Wilson & Head, 2017) predict that  
284 Phase 4 dikes had initial widths of at least 10–20 m. Cooling and solidification by  
285 conduction alone of near-stagnant magma in such dikes would occur 1-2 years after the  
286 end of an eruption.

287 In summary, the majority of the volume of magma erupted during a typical lunar  
288 eruption occurs in Phase 2 and 3 (Fig. 1a). The rise speed of magma during these phases  
289 is so large that gas bubbles stay locked to the magma, and so the vast majority of gas  
290 release into the atmosphere during a lunar eruption also occurs during Phases 2 and 3,  
291 phases that take place over about 5-10 days, less than about 25% of the total eruption  
292 duration. We now turn to a discussion of the implications of the 1) total gas release  
293 patterns and 2) gas release patterns in individual eruptions, for the formation of a  
294 transient lunar atmosphere.

295

### 296 **3 Discussion**

297 The relevant parameters (lava volume, eruption rate, duration, total gas released,  
298 gas mass release rate, etc.) for several types and scales of lunar eruptions (short flow,  
299 long flow, sinuous rille, and Cobra Head/Schroeter's Valley, the largest known lunar  
300 eruption) are shown in Table 1a. For each of the released gas masses we find the  
301 properties of the lunar atmosphere that would be created if the gas release rate from the

erupted magma was much greater than the total loss rate of the atmosphere into space by whatever mechanisms were relevant (which we shall show shortly is the case). Using the mean molecular mass  $m = \sim 31.4$  kg/kmol described above, we find the scale height of the resulting atmosphere,  $H = (Q T) / (m g)$  where  $Q$  is the universal gas constant,  $8.314$  kJ kmol<sup>-1</sup> K<sup>-1</sup>,  $T$  is the mean lunar surface temperature,  $\sim 270$  K assuming radiative equilibrium and a 25% dimmer Sun  $\sim 3.5$  Ga ago, and  $g$  is the acceleration due to gravity at the lunar surface,  $1.62$  m s<sup>-2</sup>. These values give  $H = 44.1$  km. The surface density of the atmosphere,  $\rho_s$ , is equal to its mass,  $M$ , from Table 1a, divided by the volume equivalent to the surface area of the Moon multiplied by the scale height, i.e.  $\rho_s = M / (4 \pi R^2 H)$  where  $R$  is the lunar radius,  $1738$  km. Finally, the surface pressure is  $P_s = \rho_s g H$ . Table 1b lists the values of  $\rho_s$  and  $P_s$  corresponding to the eruption types in Table 1a. Assuming the most extreme alternative volatile species mixture suggested in the literature, the sulfur-dominated mixture of Renggli et al. (2017), would increase  $m$  by a factor close to 1.5. This would decrease the scale height and increase the surface density of the atmosphere by the same factor, and leave the surface pressure unchanged.

The implied atmospheric gas masses due to the typical types of lunar volcanic activity in Table 1a are of order  $10^{12}$  to  $10^{13}$  kg. As part of an extensive review of three possible types of lunar atmosphere, Stern (1999; his section 5.2.2) treated a hypothetical volcanically-induced atmosphere with a total gas mass of  $10^{11}$  kg and adopted the loss rate calculated by Vondrak (1974) of  $10$  kg s<sup>-1</sup>. The same loss rate is estimated in a recent more general analysis by Aleinov et al. (2019) treating much more massive, at least  $\sim 10^{15}$  kg, atmospheres with surface pressures  $> 100$  Pa. Using a  $10$  kg s<sup>-1</sup> loss rate leads to the typical timescales for atmospheric decay,  $\tau_d$ , shown in Table 1b, between  $\sim 2,000$  and  $\sim 6,000$  years. These values need to be compared with the likely intervals between eruptions on the Moon. As shown earlier, with a total volume of volcanics of  $V_t = \sim 10^7$  km<sup>3</sup> (Head and Wilson, 1992; Evans, 2016), a typical erupted volume of  $200 \pm 100$  km<sup>3</sup> (Table 1a), and a total duration of volcanism of  $\tau_d = \sim 2$  Ga, the shortest average interval between eruptions is  $\sim 13,000$  to  $40,000$  years in the early part of the mare volcanism era if eruptive activity decreases with time. Increasing the 2000 ppm magmatic volatile mass fraction used here to the 3400 ppm suggested by Rutherford et al. (2017) would increase the atmospheric mass values in Table 1a by a factor of 1.7, but this would still make the timescale for atmosphere loss a factor of  $\sim 4$  less than the average time between eruptions.

What effect does the non-linear release of gas during the four phases of a typical volcanic eruption (Fig. 1a) have on the peak loss of volatiles during an eruption? To address this question, we first look at the magma volume eruption rate as a function of time for an eruption releasing  $250$  km<sup>3</sup> of magma (a medium-scale volume in the  $\sim 100$ - $300$  km<sup>3</sup> average eruption volume range described above) and lasting 46 days (about average for the 1-3 month range discussed above) (Fig. 1b). Magma volume flux is clearly highest in the first ten days (Phase 1 and 2), decreasing two orders of magnitude from an initial peak flux of  $10^6$  m<sup>3</sup> s<sup>-1</sup>, to  $10^4$  m<sup>3</sup> s<sup>-1</sup> after  $\sim 10$  days. Magma volume flux remains at this low value for the next 30 days (Phases 3-4) before falling to zero in the last 4 days at the end of the eruption. Thus,  $\sim 90\%$  of the total volume of magma erupted is emplaced in Phase 2, the hawaiian phase characterized by maximum magma degassing and volatile loss.

Using the magma volatile species proposed by Rutherford et al. (2017), the percentages of the magma, water, and CO released as a function of time in the same



348 eruption are shown in Fig. 1c. Released water closely mimics the erupted magma, unless  
349 a significant amount is left trapped in late-stage magma (Phase 4) intruded into earlier  
350 flow lobes during flow inflation. If significant inflation occurs, and the inflating gas does  
351 not escape, about 95% of the water would be released instead of 100% as shown in Fig.  
352 1c. The CO in the magma, preferentially released at very great depth, does not all escape:  
353 CO released in Phase 4 does not have time to reach the surface before the conduit freezes,  
354 even allowing for bubble coalescence and rise. However, this only represents a few  
355 percent of the total CO and so almost all of the total is released.

356 In summary, the implied intervals between typical lunar eruptions, ~13,000 to  
357 40,000 years, are 6-7 times greater than the likely durations of the vast majority of  
358 individual transient atmospheres, between ~2,000 and 6,000 years. Only for the single,  
359 extreme example of Cobra Head/Schroeter's Valley are the time scales comparable.  
360 Otherwise, only if all of the Moon's  $\sim 10^7$  km<sup>3</sup> of basaltic volcanism were to have taken  
361 place within a 300 Ma interval would the time scales generally be comparable. The non-  
362 linear release of gas during the four phases of a single eruption do not alter this  
363 conclusion; even though volatile release is concentrated in the first 25-35% of the  
364 eruption, the long repose periods between eruptions preclude sufficient buildup to create  
365 an enduring atmosphere. The same is true of leakage of gas from magma reservoirs  
366 between eruptions: if half of a typical magma volatile inventory is released uniformly  
367 over the ~40 ka average interval between eruptions, the leakage rate is somewhat less  
368 than 1 kg s<sup>-1</sup>, an order of magnitude less than the atmospheric loss rate.

369

#### 370 **4 Conclusions**

371 On the basis of our analysis of the generation, ascent and eruption of lunar mare  
372 basalt magmas and forward-modeling individual eruptions, we conclude that it is very  
373 unlikely that the Moon had a semi-permanent (as long as ~70 Ma) volcanically-driven  
374 atmosphere as proposed by Needham and Kring (2017), even during a period of peak  
375 volcanic flux in early lunar history. We attribute the differences between our estimates  
376 and those of Needham and Kring (2017) (see discussion in Supporting Material) to their  
377 use of maximum impact basin depths as average depths, and assignment of all excess  
378 volumes below datable units to one age (e.g.,  $5.9 \times 10^6$  km<sup>3</sup> assigned to 3.5 Ga in the case  
379 of Imbrium).

380 We also conclude that these low volatile release volumes and rates are not  
381 conducive to optimizing the transport of released volatiles from the eruption site to the  
382 poles to enhance the accumulation of volatiles in polar cold traps (see also Aleinov et al.,  
383 2019), nor of creating temporary environments that might favor astrobiological activity  
384 (Schulze-Makuch and Crawford, 2018). Our results suggest that most volatiles in lunar  
385 polar cold traps originated from volatile-rich impacts, rather than volatile release from  
386 volcanic eruptions, similar to findings about polar cold-trap volatile deposits on Mercury  
387 (e.g., Ernst et al., 2018; Deutsch et al., 2019, 2020). This issue could be clarified for the  
388 Moon by in situ D/H ratio measurements. In order to refine our volcanic emission  
389 estimates, future lunar exploration goals should include further analysis of detailed lava  
390 flow thicknesses, ages, volumes, volatile contents and repose periods, as well as better  
391 determination of the interior structure of mare deposits in large impact basins.

392

393 **Acknowledgements:** We gratefully acknowledge financial support from: the NASA  
394 Lunar Reconnaissance Orbiter (LRO) Mission, Lunar Orbiter Laser Altimeter (LOLA)  
395 Experiment Team (JWH); the Leverhulme Trust for funding through an Emeritus  
396 Fellowship (LW); the NASA Harriett G. Jenkins Graduate Fellowship (Grant Number  
397 80NSSC19K1289) (AND). No new data were produced or archived in this analysis.

398 **References**

- 399 Aleinov, I., Way, M. J., Harman, C., Tsigaridis, K., Wolf, E. T., & Gronoff, G. (2019). Modeling a  
400 transient secondary paleolunar atmosphere: 3-D simulations and analysis. *Geophysical Research Letters*,  
401 *46*(10), 5107-5116. <https://doi.org/10.1029/2019gl082494>  
402
- 403 Benna, M., Mahaffy, P. R., Halekas, J. S., Elphic, R. C., & Delory, G. T. (2015). Variability of helium,  
404 neon, and argon in the lunar exosphere as observed by the LADEE NMS instrument. *Geophysical Research*  
405 *Letters*, *42*(10), 3723-3729. <https://doi.org/10.1002/2015gl064120>  
406
- 407 Chen, Y., Zhang, Y., Liu, Y., Guan, Y., Eiler, J., & Stolper, E. (2015). Water, fluorine, and sulfur  
408 concentrations in the lunar mantle. *Earth and Planetary Science Letters*, *427*, 37-46.  
409 <https://doi.org/10.1016/j.epsl.2015.06.046>  
410
- 411 Cook, J. C., Stern, S. A., Feldman, P. D., Gladstone, G. R., Retherford, K. D., & Tsang, C. C. C. (2013).  
412 New upper limits on numerous atmospheric species in the native lunar atmosphere. *Icarus*, *225*(1), 681-  
413 687. <https://doi.org/10.1016/j.icarus.2013.04.010>  
414
- 415 Deutsch, A. N., Head III, J. W., & Neumann, G. A. (2019). Age constraints of Mercury's polar deposits  
416 suggest recent delivery of ice. *Earth and Planetary Science Letters*, *520*, 26-33.  
417 <https://doi.org/10.1016/j.epsl.2019.05.027>  
418
- 419 Deutsch, A. N., Head III, J. W., Parman, S. W., Wilson, L., Neumann, G. A., & Lowden, F. (2020). The  
420 mass flux of volatiles from effusive eruptions on Mercury. *Lunar and Planetary Science Conference, LI*,  
421 abstract 2259.  
422
- 423 Eke, V. R., Teodoro, L. F. A., & Elphic, R. C. (2009). The spatial distribution of polar hydrogen deposits  
424 on the Moon. *Icarus*, *200*, 12-18. <https://doi.org/10.1016/j.icarus.2008.10.013>  
425
- 426 Ernst, C. M., Chabot, N. L., & Barnouin, O. S. (2018), Examining the Potential Contribution of the  
427 Hokusai Impact to Water Ice on Mercury. *Journal of Geophysical Research*, *123*(10), 2628-2646.  
428 <https://doi.org/10.1029/2018JE005552>  
429
- 430 Evans, A. J., Soderblom, J. M., Andrews-Hanna, J. C., Solomon, S. C., & Zuber, M. T. (2016).  
431 Identification of buried lunar impact craters from GRAIL data and implications for the nearside maria.  
432 *Geophysical Research Letters*, *43*. <https://doi.org/10.1002/2015GL067394>  
433
- 434 Gaillard, F., & Scaillet, B. (2014). A theoretical framework for volcanic degassing chemistry in a  
435 comparative planetology perspective and implications for planetary atmospheres. *Earth and Planetary*  
436 *Science Letters*, *403*, 307-316. <https://doi.org/10.1016/j.epsl.2014.07.009>  
437
- 438 Hauri, E. H., Weinreich, T., Saal, A. E., Rutherford, M. C., & Van Orman, J. A. (2011), High pre-eruptive  
439 water contents preserved in lunar melt inclusions. *Science*, *333*(6039), 213-215.  
440 <https://doi.org/10.1126/science.1204626>  
441
- 442 Head III, J. W., & Wilson, L. (2017). Generation, ascent and eruption of magma on the Moon: New  
443 insights into source depths, magma supply, intrusions and effusive/explosive eruptions (part 2:  
444 observations). *Icarus*, *283*, 176-223. <https://doi.org/10.1016/j.icarus.2016.05.031>  
445
- 446 Head III, J. W., Wilson, L., Hiesinger, H., van der Bogert, C. H., Chen, Y., Dickson, J. L., et al. (2020).  
447 Lunar volcanism: Volcanic features and processes, in *New Views of the Moon (2)*, edited, in review.  
448
- 449 Head, J. W., & Wilson, L. (1981). Lunar sinuous rille formation by thermal erosion: Eruption conditions,  
450 rates and durations. *Lunar and Planetary Science Conference, XII*, 427-429.  
451
- 452 Head, J. W., & Wilson, L. (1992). Lunar mare volcanism: Stratigraphy, eruption conditions, and the  
453 evolution of secondary crusts, *Geochimica et Cosmochimica Acta*, *56*(6), 2155-2175.

- 454  
455 Hiesinger, H., Head, J. W., Wolf, U., Jaumann, R., & Neukum, G. (2011). Ages and stratigraphy of lunar  
456 mare basalts: A synthesis. In W. A. Ambrose and D. A. Williams (Eds.), *Recent Advances and Current*  
457 *Research Issues in Lunar Stratigraphy* (pp. 1-51). Geological Society of America Special Paper 477.  
458
- 459 Kring, D. A. (2014). Production of volatiles at lunar pyroclastic volcanic vents. *Annual Meeting of the*  
460 *Lunar Science Exploration Group.*, abstract 3056.  
461
- 462 Livengood, T. A., Mitrofanov, I. G., Chin, G., Boynton, W. V., Bodnarik, J. G., Evans, L. G., et al. (2018).  
463 Background and lunar neutron populations detected by LEND and average concentration of near-surface  
464 hydrogen near the Moon's poles. *Planetary and Space Science*, 162, 89-104.  
465 <https://doi.org/10.1016/j.pss.2017.12.004>  
466
- 467 Needham, D. H., & Kring, D. A. (2017). Lunar volcanism produced a transient atmosphere around the  
468 ancient Moon. *Earth and Planetary Science Letters*, 478, 175-178.  
469 <https://doi.org/10.1016/j.epsl.2017.09.002>  
470
- 471 Ni, P., Zhang, Y., Chen, S., & Gagnon, J. (2019). A melt inclusion study on volatile abundances in the  
472 lunar mantle. *Geochimica et Cosmochimica Acta*, 249, 17-41.  
473 <https://doi.org/10.1016/j.gca.2018.12.034>  
474
- 475 Newcombe, M. E., Brett, A., Beckett, J. R., Baker, M. B., Newman, S., Guan, Y., Eiler, J. M., & Stolper, E.  
476 M. (2017). Solubility of water in lunar basalt at low p<sub>H<sub>2</sub>O</sub>. *Geochimica et Cosmochimica Acta*, 200, 330-  
477 352. <https://doi.org/10.1016/j.gca.2016.12.026>  
478
- 479 Parfitt, E. A., & Wilson, L. (1995). Explosive volcanic eruptions-IX. The transition between Hawaiian-  
480 style lava fountaining and Strombolian explosive activity. *Geophysical Journal International*, 121, 226-  
481 232.  
482
- 483 Paskert, J. H., Hiesinger, H., & van der Bogert, C. H. (2015). Small-scale lunar farside volcanism. *Icarus*,  
484 257, 336-354. <https://doi.org/10.1016/j.icarus.2015.04.040>  
485
- 486 Renggli, C. J., King, P. L., Henley, R. W., & Norman, M. D. (2017). Volcanic gas composition, metal  
487 dispersion and deposition during explosive volcanic eruptions on the Moon. *Geochimica et Cosmochimica*  
488 *Acta*, 206, 296-311. <https://doi.org/10.1016/j.gca.2017.03.012>  
489
- 490 Rutherford, M. J., & Papale, P. (2009). Origin of basalt fire-fountain eruptions on Earth versus the Moon,  
491 *Geology*, 37(3), 219-222. <https://doi.org/10.1130/G25402a.1>  
492
- 493 Rutherford, M. J., Head III, J. W., Saal, A. E., Hauri, E. H., & Wilson, L. (2017). Model for the origin,  
494 ascent and eruption of lunar picritic magmas. *American Mineralogist*, 102, 2045-2053.  
495 <https://doi.org/10.2138/am-2017-5994>  
496
- 497 Saal, A. E., Chaussidon, M., Gurenko, A. A., & Rutherford, M. J. (2018). Boron and lithium contents and  
498 isotopic composition of the lunar volcanic glasses. *Lunar and Planetary Science Conference*, 49, abstract  
499 2575.  
500
- 501 Saal, A. E., Hauri, E. H., Lo Cascio, M., Van Orman, J. A., Rutherford, M. C., & Cooper, R. F. (2008).  
502 Volatile content of lunar volcanic glasses and the presence of water in the Moon's interior. *Nature*,  
503 454(7201), 192-195. <https://doi.org/10.1038/nature07047>  
504
- 505 Schulze-Makuch, D., & Crawford, I. A. (2018). Was there an early habitability window for Earth's Moon?  
506 *Astrobiology*, 18(8), 985-988. <https://doi.org/10.1089/ast.2018.1844>  
507
- 508 Shearer, C. K., Hess, P. C., Wiczorek, M. A., Pritchard, M. E., Parmentier, E. M., Borg, L. E., et al.  
509 (2006). Thermal and magmatic evolution of the moon. *Reviews in Mineralogy and Geochemistry*, 60, 365-

- 510 518. <https://doi.org/10.2138/rmg.2006.60.4>  
511  
512 Solomon, S. C., & Head III, J. W. (1980). Lunar mascon basins: Lava filling, tectonics and evolution of  
513 the lithosphere. *Reviews of Geophysics and Space Physics*, 18(1), 107-141.  
514  
515 Stern, S. A. (1999). The lunar atmosphere: History, status, current problems, and context. *Reviews of*  
516 *Geophysics*, 37(4), 453-491. <https://doi.org/10.1029/1999rg900005>  
517  
518 Vondrak, R. R. (1974). Creation of an artificial lunar atmosphere. *Nature*, 248(5450), 657-659.  
519 <https://doi.org/10.1038/248657a0>  
520  
521 Wallace, P. J., Plank, T., Edmonds, M., & Hauri, E. H. (2015). Volatiles in magmas. In H. Sigurdsson  
522 (Ed.), *The Encyclopedia of Volcanoes* (pp. 163-183). London, UK: Elsevier, Inc.  
523  
524 Weider, S. Z., Crawford, I. A., & Joy, K. H. (2010). Individual lava flow thicknesses in Oceanus  
525 Procellarum and Mare Serenitatis determined from Clementine multispectral data. *Icarus*, 209(2), 323-336.  
526 <https://doi.org/10.1016/j.icarus.2010.05.010>  
527  
528 Whitten, J. L., & Head III, J. W. (2015a). Lunar cryptomaria: Mineralogy and composition of ancient  
529 volcanic deposits. *Planetary and Space Science*, 106, 67-81. <https://doi.org/10.1016/j.pss.2014.11.027>  
530  
531 Whitten, J. L., & Head III, J. W. (2015b). Lunar cryptomaria: Physical characteristics, distribution, and  
532 implications for ancient volcanism. *Icarus*, 247, 150-171. <https://doi.org/10.1016/j.icarus.2014.09.031>  
533  
534 Wieczorek, M. A., Neumann, G. A., Nimmo, F., Kiefer, W. S., Taylor, G. J., Melosh, H. J., et al. (2013).  
535 The crust of the Moon as seen by GRAIL. *Science*, 339(6120), 671-675.  
536 <https://doi.org/10.1126/science.1231530>  
537  
538 Wilson, L., & Head III, J. W. (1981). Ascent and eruption of basaltic magma on the Earth and Moon.  
539 *Journal of Geophysical Research*, 86(B4), 2971-3001.  
540  
541 Wilson, L., & Head III, J. W. (2003). Deep generation of magmatic gas on the Moon and implications for  
542 pyroclastic eruptions. *Geophysical Research Letters*, 30(12). <https://doi.org/10.1029/2002GL016082>  
543  
544 Wilson, L., & Head III, J. W. (2017). Generation, ascent and eruption of magma on the Moon: New  
545 insights into source depths, magma supply, intrusions and effusive/explosive eruptions (Part 1: Theory).  
546 *Icarus*, 283, 146-175. <https://doi.org/10.1016/j.icarus.2015.12.039>  
547  
548 Wilson, L., & Head III, J. W. (2018). Controls on lunar basaltic volcanic eruption structure and  
549 morphology: Gas release patterns in sequential eruption phases. *Geophysical Research Letters*, 45, 5852-  
550 5859. <https://doi.org/10.1029/2018GL078327>  
551  
552 Wilson, L., Head III, J. W., & Zhang, F. (2019). A theoretical model for the formation of Ring Moat Dome  
553 Structures: Products of second boiling in lunar basaltic lava flows. *Journal of Volcanology and Geothermal*  
554 *Research*, 374, 160-180. <https://doi.org/10.1016/j.jvolgeores.2019.02.018>  
555  
556  
557 **Additional References in Supporting Material**  
558 Baker, D. M. H., & Head III, J. W. (2013). New morphometric measurements of craters and basins on  
559 Mercury and the Moon from MESSENGER and LRO altimetry and image data: An observational  
560 framework for evaluating models of peak-ring basin formation. *Planetary and Space Science*, 86, 91-116.  
561 <https://doi.org/10.1016/j.pss.2013.07.003>  
562  
563 Baker, D. M. H., & Head III, J. W. (2015). Constraints on the depths of origin of peak rings on the Moon  
564 from Moon Mineralogy Mapper data. *Icarus*, 258, 164-180. <https://doi.org/10.1016/j.icarus.2015.06.013>  
565

- 566 Baker, D. M. H., Head III, J. W., Neumann, G. A., Smith, D. E., & Zuber, M. T. (2012). The transition  
567 from complex craters to multi-ringed basins on the Moon: Quantitative geometric properties from Lunar  
568 Reconnaissance Orbiter Lunar Orbiter Laser Altimeter (LOLA) data. *J. Geophys. Res.*, *117*, E00H16.  
569 <https://doi.org/10.1029/2011JE004021>  
570
- 571 Gong, S. X., Wieczorek, M. A., Nimmo, F., Kiefer, W. S., Head III, J. W., Huang, C. L., Smith, D. E., &  
572 Zuber, M. T. (2016). Thicknesses of mare basalts on the Moon from gravity and topography. *Journal of*  
573 *Geophysical Research*, *121*(5), 854-870. <https://doi.org/10.1002/2016je005008>  
574
- 575 Head III, J. W. (1974). Orientale multi-ringed basin interior and implications for the petrogenesis of lunar  
576 highland samples. *The Moon*, *11*, 327-356, 1974.  
577
- 578 Head III, J. W. (1982). Lava flooding of ancient planetary crusts: Geometry, thickness, and volumes of  
579 flooded lunar impact basins. *The Moon and the Planets*, *26*, 61-88.  
580
- 581 Head, J. W., & Lloyd, D. D. (1971). Near Terminator Photography. *Apollo 14 Preliminary Science Report*  
582 *SP-272*, 297-300, NASA Special Publication.  
583
- 584 Hiesinger, H., Head III, J. W., Wolf, U., Jaumann, R., & Neukum, G. (2002). Lunar mare basalt flow units:  
585 Thicknesses determined from crater size-frequency distributions. *Geophysical Research Letters*, *29*(8).  
586 <https://doi.org/10.1029/2002GL014847>  
587
- 588 Horz, F. (1978). How thick are lunar mare basalts? *Proceedings 9<sup>th</sup> Lunar and Planetary Science*  
589 *Conference*, *3* (pp. 3311-3331). New York, NY: Pergamon Press, Inc.  
590
- 591 Howard, K. A., Wilhelms, D. E., & Scott, D. H. (1974). Lunar basin formation and highland stratigraphy.  
592 *Reviews of Geophysics and Space Physics*, *12*, 309-327. <https://doi.org/10.1029/RG012i003p00309>  
593
- 594 Johnson, B. C., Blair, D. M., Collins, G. S., Melosh, H. J., Freed, A. M., Taylor, G. J., et al. (2016).  
595 Formation of the Orientale lunar multiring basin., *Science*, *354*, 441-444.  
596 <https://doi.org/10.1126/science.aag0518>  
597
- 598 Lloyd, D., & Head, J. W. (1972). Orientale basin deposits (Riccioli area) in Apollo 16 earthshine  
599 photography. In *Apollo 16 Preliminary Science Report, NASA Spec. Pap., SP-315* (pp. 29-24-29-26).  
600 Washington, DC: National Aeronautics and Space Administration.  
601
- 602 Neumann, G. A., Zuber, M. T., Wieczorek, M. A., Head, J. W., Baker, D. M. H., Solomon, S. C., et al.  
603 (2015). Lunar impact basins revealed by Gravity Recovery and Interior Laboratory measurements. *Science*  
604 *Advances*, *1*, 1-10. <https://doi.org/10.1126/sciadv.1500852>  
605
- 606 Robinson, M. S., Ashley, J. W., Boyd, A. K., Wagner, R. V., Speyerer, E. J., Hawke, B. R., et al. (2012).  
607 Confirmation of sublunarean voids and thin layering in mare deposits. *Planet Space Sci*, *69*(1), 18-27.  
608 <https://doi.org/10.1016/j.pss.2012.05.008>  
609
- 610 Rutherford, M. J., Head III, J. W., Saal, A. E., Hauri, E. H., & Wilson, L. (2017). Model for the origin,  
611 ascent and eruption of lunar picritic magmas. *American Mineralogist*, *102*, 2045-2053.  
612 <https://doi.org/10.2138/am-2017-5994>  
613
- 614 Schaber, G. G. (1973). Lava flows in Mare Imbrium: Geologic evaluation from Apollo orbital  
615 photography. *Proceedings of the 4<sup>th</sup> Lunar Planetary Science Conference* (73-92).  
616
- 617 Smith, D. E., Zuber, M. T., Neumann, G. A., Lemoine, F. G., Mazarico, E., Torrence, M. H., et al. (2010).  
618 Initial observations from the Lunar Orbiter Laser Altimeter (LOLA). *Geophysical Research Letters*, *37*,  
619 L18204. <https://doi.org/10.1029/2010GL043751>  
620
- 621 Solomon, S. C., & Head III, J. W. (1979). Vertical movement in mare basins: Relation to mare

- 622 emplacement, basin tectonics and lunar thermal history. *Journal of Geophysical Research*, 84(B4), 1667-  
623 1682.
- 624
- 625 Spudis, P. D. (1993). *The Geology of Multiring Impact Basins: The Moon and Other Planets*, Cambridge  
626 University Press: Cambridge, England.
- 627
- 628 Spudis, P. D., Wilhelms, D. E., & Robinson, M. S. (2011) The Sculptured Hills of the Taurus Highlands:  
629 implication for the relative age of Serenitatis, basin chronologies and the cratering history of the Moon.  
630 *Journal of Geophysical Research*, 116, E00H03, <https://doi.org/10.1029/2011JE003903>
- 631
- 632 Stöffler, D., Ryder, G., Ivanov, B. A., Artemieva, N. A., Cintala, M. J., & Grieve, R. A. F. (2006).  
633 Cratering history and lunar chronology. *Reviews in Mineralogy and Geochemistry*, 60, 519–596.  
634 <https://doi.org/10.2138/rmg.2006.60.05>
- 635
- 636 Thomson, B. J., Grosfils, E. B., Bussey, D. B. J., & Spudis, P. D. (2009). A new technique for estimating  
637 the thickness of mare basalts in Imbrium Basin. *Geophysical Research Letters*, 36(12), L12201,  
638 <https://doi.org/10.1029/2009gl037600>
- 639
- 640 Whitten, J., Head III, J. W., Staid, M. I., Pieters, C. M., Mustard, J. F., Clark, R., et al. (2011). Lunar mare  
641 deposits associated with the Orientale impact basin: New insights into mineralogy, history, mode of  
642 emplacement, and relation to Orientale Basin evolution from Moon Mineralogy Mapper (M3) data from  
643 Chandrayaan-1. *Journal of Geophysical Research*, 116. <https://doi.org/10.1029/2010JE003736>
- 644
- 645 Whitten, J. L., & Head III, J. W. (2013). Detecting volcanic resurfacing of heavily cratered terrain:  
646 Flooding simulations on the Moon using Lunar Orbiter Laser Altimeter (LOLA) data. *Planetary and Space  
647 Science*, 85, 24-37. <https://doi.org/10.1016/j.pss.2013.05.013>
- 648
- 649 Williams, K. K., & Zuber, M. T. (1998). Measurement and analysis of lunar basin depths from Clementine  
650 altimetry. *Icarus*, 131(1), 107-122. <https://doi.org/10.1006/icar.1997.5856>
- 651
- 652 Yingst, R. A., & Head III, J. W. (1997). Volumes of lunar lava ponds in South Pole-Aitken and Orientale  
653 Basins: Implications for eruption conditions, transport mechanisms and magma source regions. *Journal of  
654 Geophysical Research*, 102(E5), 10,909-10,931.
- 655
- 656 Zuber, M. T., Smith, D. E., Watkins, M. M., Asmar, S. W., Konopliv, A. S., Lemoine, F. G., et al. (2013).  
657 Gravity field of the Moon from the Gravity Recovery and Interior Laboratory (GRAIL) Mission. *Science*,  
658 339(6120), 668-671. <https://doi.org/10.1126/science.1231507>
- 659
- 660 Zuber, M. T., Smith, D. E., Neumann, G. A., Goossens, S., Andrews-Hanna, J. C., Head, J. W., et al.  
661 (2016). Gravity field of the Orientale basin from the Gravity Recovery and Interior Laboratory Mission.  
662 *Science*, 354, 438-441. <https://doi.org/10.1126/science.aag0519>
- 663

**Table 1a.** Parameters of various types of lunar eruption. Cobra Head is the source vent of Schroeter's Valley (Head and Wilson, 2017). Released volatiles assumed to have molecular mass  $31.4 \text{ kg kmol}^{-1}$  and to form  $n = 2000$  ppm by mass of a magma that has a liquid density  $\rho_m = 3000 \text{ kg m}^{-3}$ .  $V$  = lava volume;  $F_l$  = lava volume eruption rate;  $\tau_e$  = eruption duration;  $M_g$  = total gas mass released;  $F_g$  = gas mass release rate. Typical values for parameters are quoted but individual eruption values may vary by a factor of at least 2 to 3.

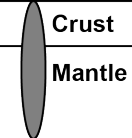
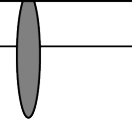
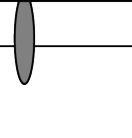
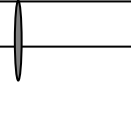
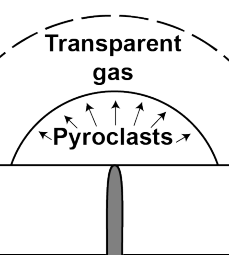
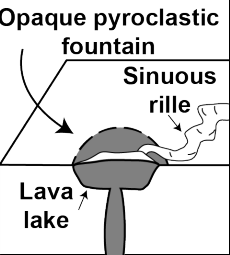
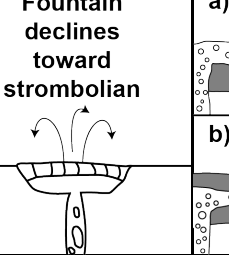
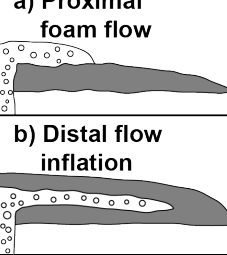
Feature	$V/\text{km}^3$	$F_l/(\text{m}^3 \text{ s}^{-1})$	$\tau_e/\text{days}$	$M_g/\text{kg}$	$F_g/(\text{kg s}^{-1})$
Cobra Head	2000	$1.4 \times 10^5$	150	$1.2 \times 10^{13}$	$9.3 \times 10^5$
Long flow	300	$\sim 10^5$	30	$1.8 \times 10^{12}$	$6.9 \times 10^5$
Small flow	200	$\sim 10^4$	100	$1.2 \times 10^{12}$	$1.4 \times 10^5$
Sinuuous rille	100	$\sim 3 \times 10^4$	50	$\sim 6 \times 10^{11}$	$1.4 \times 10^5$

**Table 1b.** Initial values of the surface density,  $\rho_s$ , and surface pressure,  $P_s$ , in a transient atmosphere produced by the four types of volcanic activity listed in Table 1a. The maximum duration of the atmosphere,  $\tau_d$ , is indicated.

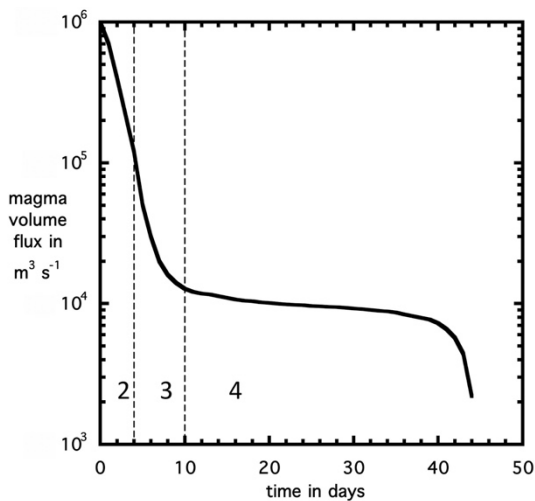
Feature	$\rho_s/(\text{kg m}^{-3})$	$P_s/\text{Pa}$	$\tau_d/\text{years}$
Cobra Head	$7.2 \times 10^{-6}$	0.51	38,000
Long flow	$1.1 \times 10^{-6}$	$7.7 \times 10^{-2}$	5,700
Small flow	$7.2 \times 10^{-7}$	$5.1 \times 10^{-2}$	3,800
Sinuuous rille	$3.6 \times 10^{-7}$	$2.6 \times 10^{-2}$	1,900



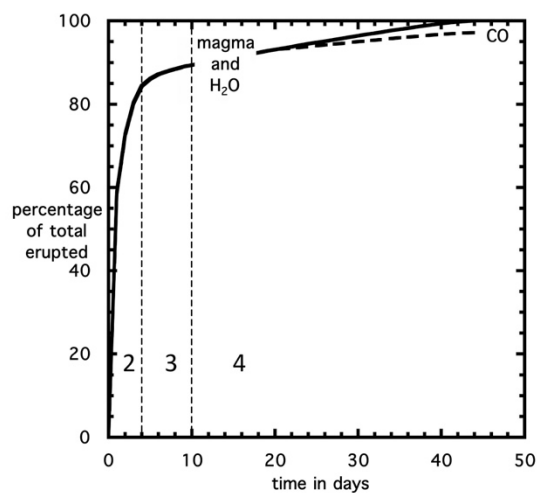
Figure 1a-c.

Eruption Phase	PHASE 1	PHASE 2	PHASE 3	PHASE 4
	Dike penetrates to surface, transient gas release phase	Dike base still rising, high flux hawaiian eruptive phase	Dike equilibration, lower flux hawaiian to strombolian transition phase	Dike closing, strombolian vesicular flow phase
Dike Configuration				
Surface Eruption Style				
Magma Rise Speed	30 to 20 m/s	20 to 10 m/s	5 to <1 m/s	< 1 m/s
Magma Volume Flux	$\sim 10^6$ m <sup>3</sup> /s	$10^6$ to $10^5$ m <sup>3</sup> /s	$10^5$ to $\sim 10^4$ m <sup>3</sup> /s	$\sim 10^4$ m <sup>3</sup> /s
Percent Dike Volume Erupted	<5%	$\sim 80\%$	$\sim 5\%$	$\sim 10\%$
Phase Duration	$\sim 3$ minutes	$\sim 4$ day	$\sim 6$ day	$\sim 30$ days

1a



1b



1c

## Supporting Material for

### “Volcanically-Induced Transient Atmospheres on the Moon: Assessment of Duration, Significance and Contributions to Polar Volatile Traps”

James W. Head<sup>1</sup>, Lionel Wilson<sup>1,2</sup>, Ariel N. Deutsch<sup>1</sup>,  
Malcolm J. Rutherford<sup>1</sup>, Alberto E. Saal<sup>1</sup>

<sup>1</sup>Department of Earth, Environmental and Planetary Sciences, Brown University,  
Providence, RI 02912 USA.

<sup>2</sup>Lancaster Environment Centre, Lancaster University, Lancaster LA1 4YQ UK.

#### Analysis and Assessment of Procedures and Assumptions:

In this supplementary material, we provide commentary on the major sources of uncertainty in assessing the duration and significance of volcanically-induced transient atmospheres and major sources of uncertainty in the approach, as a guide for comparison to our forward-model gas exsolution estimates in the main text. We summarize the procedures and assumptions used by Needham and Kring (2017) (N&K) to determine the mare basalt volcanic flux that, together with their volatile exsolution model, is the input into their lunar atmospheric buildup and retention calculations (Fig. S1). We also discuss how future work could help improve these estimates.

Major steps in establishing the atmospheric buildup and retention include 1) estimating the mare basalt volume, (2) determining the mare basalt volcanic flux (volume as a function of time), and (3) estimating the production of lunar volatiles over time.

#### S1. Estimating the mare basalt volume in each basin

In order to estimate the total volume of basalt erupted with time, N&K first tabulate the volumes of basalts erupted into each of the major impact basins (e.g., Imbrium, Serenitatis, etc.) or areas of accumulation (e.g., Oceanus Procellarum) (N&K, their Table 1). There are various levels of uncertainty pertaining to basin size (assignment of rings in multi-ring basins), the initial and final basin geometry, and the state of degradation and response to the thermal structure of the Moon at the time of basin formation that influence estimates of basalt volume in any particular basin. As discussed by N&K, there is also a high level of uncertainty in past estimates of the total thickness and volumes of mare basalts in individual basins using different techniques (e.g., Crisium basin estimates differ by  $5 \times 10^5 \text{ km}^3$ ).

For most of the major mare basins (in order of decreasing total volume: Imbrium, Serenitatis, Crisium, Humorum, Nectaris, Grimaldi, Smythii), N&K use the *basin depth-diameter estimates* of Williams and Zuber (1998) as input into their maximum thickness estimates for their volume calculations; they describe these as generally consistent with the more recent data from LOLA and GRAIL. N&K augment this with older data (Horz, 1978: Procellarum, Tranquillitatis; Yingst and Head, 1997: South Pole-Aitken) and a more recent study for Orientale (Whitten et al., 2011). These data then represent the

45 values for the total mare basalt fill thickness in each of eleven lunar basins (N&K, their  
46 Table 1) (Fig. S2a).

47 One source of uncertainty with this approach is that the Williams and Zuber (1998)  
48 estimates for impact basin geometry and lava fill thicknesses were compiled with low  
49 resolution Clementine altimetry data. In addition, N&K make several assumptions about  
50 the initial structure of the basins, and together, these factors tend to very significantly  
51 overestimate the total basin volumes in several key cases (e.g., Imbrium, Serenitatis).  
52 The Williams and Zuber (1998) maximum thickness estimates (N&K, their Table 1,  
53 column 3) are then used by N&K as *average thicknesses* to compute the entire mare  
54 basalt volume in each of the 11 basins treated by Williams and Zuber (1998) (N&K, their  
55 Table 1, column 4). These 11 total volumes (N&K, their Table 1, column 4) then account  
56 for 44% of the lunar separate mare accumulation *areas* considered (11 of 25), but >95%  
57 of the total global mare basalt *volume* calculated by N&K (Fig. S2b).

58 More specifically, the Williams and Zuber (1998) approach to estimating maximum  
59 basalt thickness in each basin is as follows: Clementine LIDAR data are used to calculate  
60 the depths of 29 large craters and basins on the Moon; the most well-preserved examples,  
61 generally unflooded by mare basalt volcanism, are then compared with previous  
62 depth/diameter (d/D) plots, revealing an inflection point in the diameter range  
63 characterized by the transition from complex craters to peak-ring basins.

64 From this relationship, an empirical power law fit is derived for basin depth as a  
65 function of increasing size, a relationship characterized by a shallower slope than that of  
66 complex craters. The definition of this inflection point is provided by seven peak-ring  
67 basins ranging in diameter from 100-200 km. Williams and Zuber (1998) then use this  
68 empirical power law basin-scale d/D relationship to estimate the thickness of mare basalt  
69 fill in each basin by assuming that the unfilled depths of each basin follow this d/D  
70 relationship, and the current mare fill elevation represents the upper bound on the  
71 thickness. Thus, the Williams and Zuber (1998) estimated basalt thicknesses for each  
72 basin are derived from “the difference between the predicted basin depth and the  
73 measured depth of the mare surface.” N&K then use these Williams and Zuber (1998)  
74 thickness estimates (N&K, their Table 1, column 3) as input to their basin volume  
75 calculations.

76 Among the sources of uncertainty in the thickness estimates derived by Williams and  
77 Zuber (1998) are:

- 78 1. Loading and flexure of the basin interior can cause basin subsidence (e.g.,  
79 Solomon and Head, 1979, 1980), resulting in mare basalt thickness in the basin  
80 interior being greater than that predicted by the d/D relationship. Williams and  
81 Zuber (1998) accounted for this loading-related subsidence in their calculations  
82 (their Table 2), and thus this is accounted for in the thicknesses N&K utilize in  
83 their Table 1.
- 84 2. Not all of the basins chosen by N&K to apply the Williams and Zuber (1998)  
85 thickness estimates to derive volumes (the 11 basins in their Table 1) were  
86 comparable to the most well-preserved and generally unmodified basins used to  
87 calculate the empirical power-law fit. A large number of factors can influence  
88 basin topography during and subsequent to basin formation: initial lithospheric  
89 thermal structure, subsequent viscous relaxation, and impact-induced  
90 topographic degradation are all likely to mean that older basins (for example,

91 old Tranquillitatis compared with young Imbrium) were shallower than the  
 92 empirical fit when they began to be filled with mare basalt, resulting in  
 93 overestimation of the thickness of their fill. Impact degradation can lower rim  
 94 elevation, emplace ejecta inside the basin, and shallow the floor, all decreasing  
 95 the basin depth prior to filling with mare basalt. For example, the impact event  
 96 forming the Imbrium basin emplaced significant thicknesses and volumes of  
 97 ejecta inside the Serenitatis basin (Spudis et al., 2011), volumes that would need  
 98 to be subtracted from the total thickness, and thus volume, of Serenitatis mare  
 99 fill.

- 100 3. Scaling depth/diameter relationships to larger basin-scale diameters implies a  
 101 consistent choice for the crater and basin diameter. Unfortunately, the choice of  
 102 which ring in multi-ring basins represents the closest approximation to the crater  
 103 or peak-ring basin rim crest is controversial (see Head, 1974; Howard et al.,  
 104 1974; Spudis, 1993; Neumann et al., 2015; Zuber et al, 2016; Johnson et al.,  
 105 2016, for discussion of this problem) and thus the choice of basin diameter to  
 106 input into the extrapolation of depth/diameter relationships to larger basin-scale  
 107 diameters could vary by several tens of percent.
- 108 4. Depth/diameter relationships provide data on the *maximum* depth of the basin,  
 109 and thus the *maximum* thickness of the fill, not the *average* thickness. For  
 110 example, the Orientale basin has a maximum depth of >8 km but the majority of  
 111 the basin is less than ~2 km deep (Fig. S3a). The geometry of the interior of  
 112 multi-ringed basins differs significantly from a cylindrical plug (Fig. S3b). For  
 113 example, the thickness of mare basalts may differ by a factor of four between  
 114 the deepest part of the basin interior and the outer area overlying the terrace  
 115 inside the topographic ring. Volcanic flooding models of the essentially  
 116 unfilled Orientale basin (Head, 1982) showed that the area between the Inner  
 117 Rook ring and the Cordillera ring, an area making up more than 70% of the total  
 118 area of the basin, had lava thicknesses of less than 2 km, a thickness about 25%  
 119 of the deepest part of the basin.
- 120 5. There are uncertainties in extrapolating d/D data from the diameter range of  
 121 peak-ring basins to the much larger scale of multi-ringed basins. Using much  
 122 improved d/D data from the Lunar Orbiter Laser Altimeter (Smith et al., 2010)  
 123 and GRAIL gravity data (Zuber et al., 2013), Baker and Head (2013) and Baker  
 124 et al. (2012) showed that there is a possible further shallowing of the slope of  
 125 the d/D trend at the multi-ringed basin scale, the diameter of most of the 11  
 126 basins considered by Williams and Zuber (1998) and N&K. This predicted  
 127 shallowing would result in the thicknesses calculated by the Williams and Zuber  
 128 (1998) method (N&K, their Table 1, column 3) being overestimates.

129 *Summary of the N&K tabulation of mare basalt volumes in the 11 major mare basins:* In  
 130 order to derive the total volume of mare basalt in each basin, N&K use the *maximum*  
 131 *thickness* estimates of William and Zuber (1998) (N&K, their Table 1, column 3). They  
 132 assume that this is the *average thickness* (Fig. S3b), and multiply this maximum  
 133 thickness by the area inside the basin to derive a *total volume of mare basalt in each*  
 134 *basin* (N&K, their Table 1, column 4). For example, in the Imbrium basin, N&K use the  
 135 thickness of mare basalts determined by Williams and Zuber (1998) derived as follows  
 136 (Fig. S3b: Imbrium basin extrapolated d/D, minus depth to current mare surface, yields a

137 thickness of 4.70 km; adjusting this for loading and subsidence yields a *maximum*  
 138 thickness of 5.24 km for the lava at the center of the Imbrium basin. N&K then take this  
 139 *maximum* thickness, which includes all of the caveats described above predicting that the  
 140 sign of this value will be an overestimate, and then take two additional steps: 1) they  
 141 calculate the area of the Imbrium basin to cover 1,010,400 km<sup>2</sup>, and then assume that the  
 142 *maximum* thickness estimate of 5.24 km is the *average* thickness over the entire  
 143 1,010,400 km<sup>2</sup> area of the basin, yielding a *total volume* of the Imbrium basin mare fill to  
 144 be 5.295 x 10<sup>6</sup> km<sup>3</sup> (Fig. S3b). On the basis of using a *maximum* thickness estimate  
 145 (very likely to be an overestimate for the reasons stated above) and assuming that it  
 146 represents the *average* thickness for the whole basin, we believe that this value  
 147 *significantly overestimates* the volume of mare basalt in the Imbrium basin. A similar  
 148 approach is utilized for each individual basin (N&K Table 1) suggesting that these values  
 149 will also be overestimates.

150

### 151 ***S1.1 Opportunities and prospects for current and future improved estimates***

152 The major uncertainties in the total volume estimates for each basin derive from lack  
 153 of detailed knowledge of the underlying geometry of impact basins at the time of their  
 154 initial mare fill, and their detailed response to topographic filling (loading, flexure and  
 155 subsidence). New Lunar Orbiter Laser Altimeter (LOLA) and Gravity Recovery and  
 156 Interior Laboratory (GRAIL) data are the types of data that can help reduce this  
 157 uncertainty. The acquisition of much higher resolution altimetry data (Lunar Orbiter  
 158 Laser Altimeter; Smith et al., 2010) and gravity data (GRAIL; Zuber et al., 2013)  
 159 permitted better understanding of the topography of craters, peak-ring and multi-ring  
 160 basins (e.g., Baker and Head, 2013, 2015) and an understanding of the three-dimensional  
 161 structure and lava filling histories of impact craters and basins. For example, Whitten  
 162 and Head (2013) provided detailed modeling of lava flooding and progressive filling  
 163 estimates for typical peak-ring basins and degraded multi-ring basins. Evans et al. (2016)  
 164 used GRAIL gravity data to assess the presence of craters buried by lava filling and the  
 165 thickness and volume of their fill. LOLA and GRAIL data have also been used to  
 166 estimate the average thicknesses of mare basalts on the lunar nearside (0.74 km) (Gong et  
 167 al., 2016). For the future, there is a compelling need for detailed basin-wide geophysical  
 168 traverse surveys to assess the depth to the mare-basin floor interface, the depth and  
 169 geometry of the crust-mantle interface, and variations in basin geometry and fill as a  
 170 function of initial basin age.

171

### 172 **S2. Determining the mare basalt volcanic flux (volume of lava extruded as a** 173 **function of time)**

174 To convert total estimated mare basalt volumes derived for each basin (as described  
 175 above) into a volcanic flux (volume as a function of time), the ages of the various mare  
 176 basalt units need to be determined and their relative abundance assessed. Six steps are  
 177 needed to accomplish this task: 1) definition of a volcanic unit, and then determination of  
 178 the 2) area covered by the unit, 3) thickness of the unit, 4) volume of the unit, 5) age of  
 179 the unit, and finally, 6) duration of its emplacement. Obviously, deriving each of the six  
 180 factors in these estimates becomes more and more difficult for older and older deposits,  
 181 as the stratigraphically younger flow units mask the older flow units (Fig. S4). Needham  
 182 and Kring (2017) use the following set of steps to accomplish this task:

183 ***S2.1. Estimate mare unit area and age***

184 N&K use the mare unit boundary mapping and crater size frequency analyses data  
185 from Hiesinger et al. (2011) (and others). On the basis of these data they conclude that  
186 mare basalt provinces were emplaced from ~3.9 Ga to as recently as ~1.1 Ga.

187 ***S2.2. Estimate mare unit thickness***

188 N&K note that “observations of specific mare eruptive units indicate an average mare  
189 unit thickness of ~250 m (Weider et al., 2010) within Serenitatis and Oceanus  
190 Procellarum...” with this thickness “...expected to incorporate an integrated sequence of  
191 thinner flows....and is assumed to be the average thickness for all surface mare units in  
192 the absence of other thickness measurements...” In the analysis of Weider et al. (2010),  
193 they identify eight units (their Table 4) with estimated average unit thicknesses ranging  
194 from 80-600 m, and derive an average of 250 m derived by averaging the total of the  
195 individual values in their Table 4.

196 As N&K acknowledge, spectrally defined flow units can easily be composed of  
197 multiple lava flows of similar composition. In addition, the thickness of a flow unit is  
198 related to the nature of the underlying topography: flows emplaced in rough terrain such  
199 as the interior of craters or the highlands will pond and be much thicker than flows  
200 emplaced on a flat or sloping mare plain (e.g., Head, 1982; Whitten and Head, 2013). A  
201 wide range of mare basalt flow and unit thickness have been observed or inferred in the  
202 relatively flat lunar maria, as follows: 1) 3-5 m from near-terminator images of flow  
203 fronts (Head and Lloyd, 1971; Lloyd and Head, 1972); 2) average of 30-35 m in the flow  
204 fronts in the observed young Eratosthenian-aged flow fronts in Mare Imbrium (Schaber,  
205 1973); 3) 30-60 m average thickness (range of 20-220 m) from basalt flow units exposed  
206 within the nearside maria, using inflections in impact crater size-frequency distributions  
207 (Hiesinger et al., 2002); 4) ~10 m average flow thicknesses estimated from exposed  
208 sections in impact crater and pit crater walls (Robinson et al., 2012).

209 On the basis of these estimates, all typically less than ~50 m, we conclude that the  
210 average thickness of 250 m may overestimate the average thickness of individual lava  
211 flows by a factor of five. Clearly, average thickness in the initial rough topography of  
212 the basin floor may have been larger, but as shown by the interior of Orientale (e.g.,  
213 Head, 1982; Whitten et al., 2011), these variations will soon tend to smooth out due to  
214 emplacement of superposed lavas. An additional factor is that a spectrally defined lava  
215 flow unit may be composed of a series of individual lava flows. The values determined  
216 by Weider et al. (2010) are for spectrally defined flow units, and thus these are likely to  
217 be composed of a series of flow units whose thickness was cumulative. Using this  
218 average 250 m flow thickness to estimate the thickness of all previous dated flow units  
219 carries with it the interpretation that these previously dated flow units are likely to be  
220 composed of multiple flow units of uncertain age range. This is acknowledged by N&K,  
221 but needs to be kept in mind as one moves forward to the determination of volatile flux in  
222 individual eruptions and the contribution of such individual eruptive events to production  
223 and retention of a transient atmosphere. For example, if a dated 250 m thick lava flow  
224 unit consists of five separate 50 m thick eruptive lava flows, what are the thicknesses,  
225 volumes and volatile fluxes of each of the individual eruptions, and is the repose period  
226 between their emplacement sufficient to cumulatively contribute to the buildup of a  
227 transient atmosphere, or do the volatiles dissipate between eruptions?  
228

### 229 ***S2.3 Estimate mare basalt erupted volume as a function of time***

230 Step 1: Surface Flows: Needham and Kring (2017) then used the individual mapped  
 231 mare basalt units and ages (predominantly from Hiesinger et al., 2011) to calculate the  
 232 volume of surface mare basalts emplaced in each basin as a function of time (their Fig.  
 233 2a; reproduced as Fig. S1a). These mapped and dated mare units are exposed at the  
 234 surface, and thus overlie older units for which only relative ages are available (they are  
 235 older because they underlie the basalts exposed at the surface) (Fig. S4).

236 Step 2: Lava Flows Underlying Exposed Surface Flows: Needham and Kring then  
 237 “assume that the underlying flows were emplaced as older surface flows that were  
 238 embayed by younger surface flows, such that the mare units are stacks of superposed lava  
 239 units emplaced via effusive surface eruptions. Although ages of underlying basalts, with  
 240 volumes taken as the difference between the total mare basalt for a given basin and the  
 241 volume of the mapped surface flows, are not identified directly, these deposits are at least  
 242 as old as the oldest surface unit (noted in italics in their Table S1).” (Fig. S4). Without  
 243 age constraints on the underlying units, it is not possible to accurately describe the timing  
 244 of the older eruptions. N&K provide a maximum estimate by assuming that all  
 245 underlying units erupted at the same time as the surface units.

246 These underlying units are then dealt with by Needham and Kring in two ways as  
 247 shown in the following example for the Imbrium basin:

- 248 1. The oldest dated mare unit in the Imbrium basin is listed as 3.55 Ga (their Table  
 249 S1). For the basin maria “with unreported ages of units or of units underlying  
 250 surface mare with identified ages” (their Table S1 explanation, italicized entries  
 251 as listed in Table S1), N&K assign an age to these *undated and underlying units*  
 252 that is equal to the age of the oldest flow (3.55 Ga). For Imbrium, this gives 17  
 253 units that are 3.55 Ga, the age of the oldest dated flow, adding an additional  
 254 25,383 km<sup>3</sup> of lava emplaced at this age (3.55 Ga). This provides a total volume  
 255 of “dated flows” (35 basalt units ranging in age from 1.1 to 3.5 Ga with a  
 256 volume of 221,217 km<sup>3</sup>, 4.3% of the total Imbrium basin mare fill of 5,294,497  
 257 km<sup>3</sup>), plus unreported and underlying surface units (17 units, all assigned the  
 258 age of the oldest dated unit, 3.55 Ga with a volume of 25,383 km<sup>3</sup>, 0.5% of the  
 259 total Imbrium basin mare fill) (summarized as percentages in parentheses in Fig.  
 260 S4). An exact definition of the “underlying units” is not provided, but it  
 261 consists of these 17 units (their Table S1, units with ages in italics).
- 262 2. In order to account for the rest of the mare basalt basin fill that lies below the  
 263 dated flows, the undated flows together with the “underlying units”, N&K take  
 264 the total volume of these flow units (35 + 17 = 52 units in the case of the  
 265 Imbrium basin) and subtract this number (252,600 km<sup>3</sup>) from their total volume  
 266 of the Imbrium basin derived from using the Williams and Zuber (1998)-based  
 267 thickness estimate (N&K, their Table 1, column 3) to derive a *total volume*  
 268 *estimate* (5,294,497 km<sup>3</sup>; N&K, their Table 1, column 4), thus identifying  
 269 5,041,900 km<sup>3</sup> of additional basin fill (95.2% of the total Imbrium basin  
 270 volume) as “excess volume”. They then assign all of this remaining “excess  
 271 volume” (95.2% of the total Imbrium basin fill) to an age of the oldest dated  
 272 surface flow (3.55 Ga), resulting in 95.2% of the total Imbrium basin fill having  
 273 a single age (Fig. S4).

274 *Summary:* In summary, N&K take the total Imbrium basin volume from the Williams



275 and Zuber (1998) maximum basalt thickness estimate, assume that it represents the  
 276 average mare fill thickness in the basin (Fig. S3b), and then subtract the volumes that  
 277 they have accounted for so far with “dated surface”, “undated surface” and “subsurface”  
 278 flow units (4.8% of the total Imbrium basin volume), and subtract this total number from  
 279 the “grand total” implied by adopting the Williams and Zuber number maximum  
 280 thickness number as the average thickness number. N&K then assign *all of this*  
 281 remaining “excess volume” (95.2% of the total volume) to an age of emplacement of the  
 282 *oldest dated surface flow*, 3.55 Ga (Fig. S2c, S4). This 95.2% of their estimated total  
 283 basin volume accounts for virtually all of the  $\sim 5.4 \times 10^6 \text{ km}^3$  peak in global mare basalt  
 284 flux at  $\sim 3.55$  Ga shown in N&K Figure 2a (Figure S1a).

285 N&K treat the second largest basin fill volume (the Serenitatis basin) in a similar  
 286 manner (Fig. S2d). The total Serenitatis basin volume is derived by N&K using the  
 287 maximum thickness from Williams and Zuber (1998) as an average thickness (Fig. S3b)  
 288 (N&K, their Table 1, column 3), multiplying by the total basin area (N&K, their Table 1  
 289 column 2), to obtain a total basin mare basalt volcanic fill volume of  $1,473,679 \text{ km}^3$   
 290 (N&K, their Table 1, column 4). They define 23 dated basin units, ranging in age from  
 291 2.44-3.81 Ga, that make up a volume of  $62,262 \text{ km}^3$ , 4.2% of the total. They further  
 292 identify 12 additional units comprised of “undated surface” and “subsurface” flow units,  
 293 that make up a volume of  $23,417 \text{ km}^3$ , 1.6% of the total Serenitatis basin, and add this to  
 294 the 23 dated flows, for a total of  $85,679 \text{ km}^3$ , a volume making up 5.8% of the total  
 295 Serenitatis basin volume estimated by N&K (column 4, their Table 1). Finally, they  
 296 subtract this subtotal from the volume “grand total” derived from using the Williams and  
 297 Zuber maximum thickness number as an average thickness ( $1,473,679 \text{ km}^3$ ; their Table 1  
 298 column 4), yielding an ‘excess volume’ of  $1,388,000 \text{ km}^3$ , 94.2% of the total volume in  
 299 the Serenitatis basin. This entire “excess volume” is then assigned the age of the oldest  
 300 dated flow, 3.81 Ga, resulting in  $\sim 94\%$  of the total volume in the Serenitatis basin (N&K,  
 301 their Table 1, column 4) being assigned to a single emplacement age (3.81 Ga) (Fig.  
 302 S2d). This 94.2% accounts for virtually all of the  $\sim 1.5 \times 10^6 \text{ km}^3$  peak in global mare  
 303 basalt flux at  $\sim 3.8$  Ga shown in Needham and Kring Figure 2a (Figure S1a).

304 *Implications:* The assignment of this huge “excess volume” in individual basins  
 305 (95.2% of the total Imbrium basin mare basalt volume; 94.2% of the total Serenitatis  
 306 basin mare basalt volume) to one specific age (Imbrium = 3.55 Ga; Serenitatis = 3.81 Ga)  
 307 then forms almost the entire  $5.5 \times 10^6 \text{ km}^3$  global peak in the mare basalt flux at 3.5 Ga  
 308 seen in their Figure 2a and the second peak at  $\sim 3.8$  Ga in their Figure 2a (Fig. S1a).

309

#### 310 ***S2.4 Opportunities and prospects for current and future improved estimates of mare*** 311 ***basalt age assignments and total volumes (flux)***

312 What are the alternative approaches to the N&K assignment of the huge “excess  
 313 volume” to the age of the single oldest dated flow? Instead of assigning 95.2% of the  
 314 undated volume in Imbrium to one age one could spread this volume evenly out over the  
 315 entire time between the approximate formation of the Imbrium basin (about 3.85 Ga; see  
 316 discussion in Stoffler et al., 2006), and the 3.55 age (oldest dated surface flow), reducing  
 317 the peak down to  $< 2 \times 10^6 \text{ km}^3$ , spread out over 250-300 Ma (compare this to their Fig.  
 318 2a; Fig. S1a here). In another approach, Thompson et al. (2009) used superposed craters  
 319 penetrating through the mare basalt to derive a total volume for the Imbrium basin mare  
 320 basalt fill of  $1.3 \times 10^6 \text{ km}^3$ . The Thompson et al. (2009) value is only  $\sim 25\%$  of the

321 Needham and Kring total volume value ( $5.295 \times 10^6 \text{ km}^3$ ). Future exploration to address  
 322 this uncertainty should involve a sample return mission to the ejecta of crater penetrating  
 323 the entire mare fill, and regional geophysical surveys to establish subsurface stratigraphy  
 324 and structure.

325

### 326 **S3. Production of Lunar Volatiles Over Time**

327 N&K now take the total “Volume of erupted basalts as a function of time, indicating  
 328 peak volcanic activity primarily in the Imbrium basin ca. 3.5 Ga.” (their Fig. 2a; Fig. S1a  
 329 here) and calculate the “Mass of volatiles, primarily CO and S, degassed during mare  
 330 emplacement...” (their Fig. 2b; our Fig S1b here). In order to convert the mare basalt  
 331 fluxes, as discussed above, to a production function for volatiles released over time, N&K  
 332 first estimate the proportion of volatiles degassed during mare emplacement (their Table  
 333 2), using maximum and minimum values reported in the literature for five species (CO,  
 334 H<sub>2</sub>O, H<sub>2</sub>, OH and S). They then estimate the percent of each gas species liberated from a  
 335 unit mass (CO, 100%; H<sub>2</sub>O, 90%; H<sub>2</sub>, 100%; OH, 99%; S, 90%), and then convert this to  
 336 maximum and minimum degassed masses of gas for each species in ppm (their Table 2).  
 337 The “mass of erupted lava was then calculated by multiplying the estimated volume by  
 338 the bulk density of typical mare basalt ( $\sim 3.00 \text{ g/cm}^3$ ).” and this mass was then multiplied  
 339 by the minimum and maximum contents of each mare basalt volatile species as listed in  
 340 their Table 2. This approach enabled the determination of “the mass range of each  
 341 volatile released during an eruption”.

342 The next step taken by Needham and Kring was to assess “Incremental production...  
 343 calculated for mare volumes erupted every 0.1 Ga.” Their Table S3 shows that a grand  
 344 summed total of  $8,900,775 \text{ km}^3$  of mare lava was erupted on the Moon; 61.2% of this  
 345 total ( $5,446,355 \text{ km}^3$ ) was erupted at the 100 Ma interval centered at 3.5 Ga, and of this  
 346 61.2%, 93.5% was erupted in the Imbrium basin. Finally, 99.5% of this total erupted  
 347 volume was “undated” and “excess” lava, underlying the four oldest dated flow units in  
 348 Imbrium (3.5-3.55 Ga,  $24,031 \text{ km}^3$ ) (Fig. S2c): on the basis of Needham and Kring  
 349 approach outlined above, all of this 99.5% was assigned the age of the oldest flow, 3.5  
 350 Ga.

351 Their Table S3 also shows that, of the grand summed total of  $8,900,775 \text{ km}^3$  of mare  
 352 lava erupted on the Moon, 17% of this total ( $1,525,044 \text{ km}^3$ ) was erupted in the 100 Ma  
 353 interval centered at 3.8 Ga, and of this 17%, 92.6% was erupted in the Serenitatis basin.  
 354 Finally, 99.5% of this total volume erupted in Serenitatis was “undated” and “excess”  
 355 lava, underlying the oldest dated flow unit in Serenitatis (3.85 Ga,  $621 \text{ km}^3$ ) (Fig. S2d):  
 356 on the basis of N&K approach outlined above, all of this 99.5% was assigned the age of  
 357 the oldest flow, 3.85 Ga.

358 Needham and Kring then use these data in order to derive the “Mass and surface  
 359 pressure of volatiles degassed by lunar mare basalt as a function of time“ (their Table  
 360 S3). The results are plotted in their Figure 2c (Fig. S1c here), the “Atmospheric surface  
 361 pressure resulting from the volatiles released during mare emplacement, with a peak  
 362 pressure  $\sim 1\%$  of Earth’s current atmospheric pressure corresponding to peak volcanic  
 363 activity 3.5 Ga.”

364 *Summary:* On the basis of this assessment and analysis, the Needham and Kring  
 365 approach of assigning the “underlying”, “undated” and “excess” mare lavas to a single  
 366 age (the age of the oldest flow) (Fig. S4), and the reservations outlined above concerning

367 the use of the “maximum” basin depth from Williams and Zuber (1998) as an “average  
 368 depth” for the mare fill, appear to create unrealistically large volumes focused at single  
 369 time intervals (3.5 Ga for Imbrium and 3.8 for Serenitatis), that tend to produce and  
 370 significantly overestimate the peak flux at these times (their Figure 2b; Fig. S1b here). In  
 371 a final step, the resulting production functions were then plotted (their Figure 2b; Fig.  
 372 S1b here) and were summarized in their Table S3. Needham and Kring conclude that  
 373 these data clearly show that peak volatile releases occurred at 3.8 Ga and 3.5 Ga.

374 Among the uncertainties in this approach, in addition to the total volumes and age  
 375 assumptions for individual basins discussed above, are:

376 1) Eruption time period (duration): Volcanic unit ages, volumes, and gas release  
 377 masses are binned in 100 Ma intervals (N&K, their Table S3). This binning effectively  
 378 serves to reduce any individual eruptive peaks to an average of the 100 Ma period. If the  
 379 volumes of units and their individual ages were known with great accuracy, an individual  
 380 peak could potentially greatly exceed the average, and its contribution to a lunar  
 381 atmosphere could be underestimated.

382 2) Time-dependent volatile input during a single eruption: Gas release during  
 383 volcanic eruptions is typically non-linear, decreasing as a function of time during the  
 384 eruption. Depending on the eruption duration, this could have a significant effect on the  
 385 volumetric contributions of volatiles to an atmosphere and its dissipation history.  
 386 Similarly, individual gas species vent at different rates and times during eruptions,  
 387 important considerations in potential buildup and retention in an atmosphere. We treat  
 388 these factors in more detail in the main contribution.

389 3) Eruption repose period (time between eruptions): Similarly, summing the entire  
 390 volume and flux for a 100 Ma period implies that this input was continuous into the  
 391 atmosphere for a 100 Ma period. If the repose period was significant, the atmospheric  
 392 contribution from a single event may completely dissipate, rather than contribute to the  
 393 buildup from a longer term average input. The  $\tau_d$  values in our Table 1b in the main text  
 394 show that (ignoring the one-off Cobra Head event), two eruptions would have to occur  
 395 within ~4000 years of one another for there to be a significant effect on prolonging a  
 396 temporary atmosphere. Approximating the 20,000 to 60,000 year typical interval by  
 397 normal distribution with mean 40,000 and standard deviation 20,000, a 4000 year interval  
 398 would have a probability of ~3%.

399

### 400 ***S3.1 Opportunities and prospects for current and future improved estimates of mare*** 401 ***basalt volatile contributions to an atmosphere***

402 Clearly, improved stratigraphic relationships of dated lava flows in the most  
 403 volumetrically significant lunar basins (e.g., Imbrium, Serenitatis) would be essential to  
 404 decreasing the uncertainty in the Needham and Kring (2017) estimates, as would more  
 405 precise determinations of the absolute ages of individual lunar basins. Also critically  
 406 important is the initial volatile content of mare basalt magmas generated at depth and  
 407 their global variability, as well as volatile release (e.g., Rutherford et al., 2017) and loss  
 408 processes as a function of individual eruptions (e.g., Wilson and Head, 2018).  
 409 Information on volumes of individual eruptions, their duration, and the chronology of  
 410 volatile speciation and loss would be essential for the reliable determination of loss rates  
 411 and contributions to a candidate lunar atmosphere.

412

413 **References:**

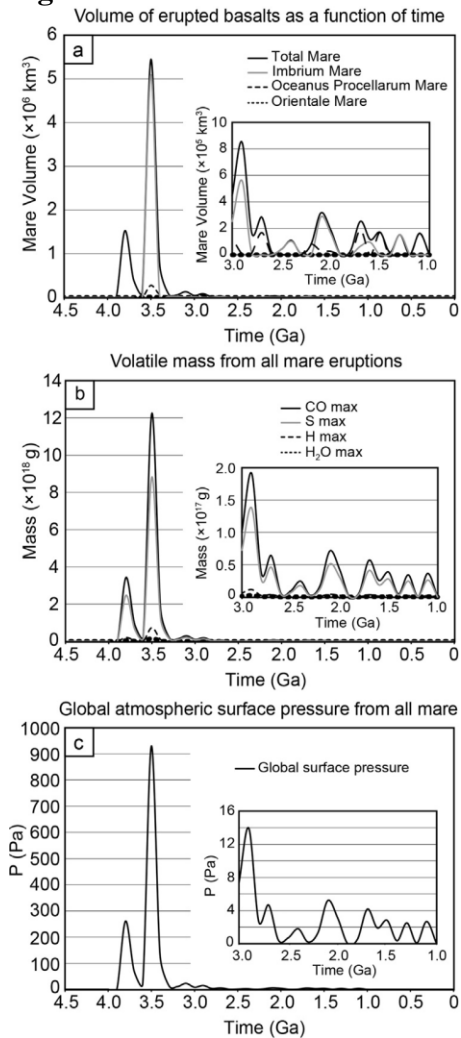
- 414 Baker, D. M. H., & Head III, J. W. (2013). New morphometric measurements of craters and basins on  
 415 Mercury and the Moon from MESSENGER and LRO altimetry and image data: An observational  
 416 framework for evaluating models of peak-ring basin formation. *Planetary and Space Science*, 86, 91-116.  
 417 <https://doi.org/10.1016/j.pss.2013.07.003>  
 418
- 419 Baker, D. M. H., & Head III, J. W. (2015). Constraints on the depths of origin of peak rings on the Moon  
 420 from Moon Mineralogy Mapper data. *Icarus*, 258, 164-180. <https://doi.org/10.1016/j.icarus.2015.06.013>  
 421
- 422 Baker, D. M. H., Head III, J. W., Neumann, G. A., Smith, D. E., & Zuber, M. T. (2012). The transition  
 423 from complex craters to multi-ringed basins on the Moon: Quantitative geometric properties from Lunar  
 424 Reconnaissance Orbiter Lunar Orbiter Laser Altimeter (LOLA) data. *J. Geophys. Res.*, 117, E00H16.  
 425 <https://doi.org/10.1029/2011JE004021>  
 426
- 427 Evans, A. J., Soderblom, J. M., Andrews-Hanna, J. C., Solomon, S. C., & Zuber, M. T. (2016).  
 428 Identification of buried lunar impact craters from GRAIL data and implications for the nearside maria.  
 429 *Geophys. Res. Lett.*, 43, 2445-2455. <https://doi.org/10.1002/2015GL067394>  
 430
- 431 Gong, S. X., Wieczorek, M. A., Nimmo, F., Kiefer, W. S., Head III, J. W., Huang, C. L., Smith, D. E., &  
 432 Zuber, M. T. (2016). Thicknesses of mare basalts on the Moon from gravity and topography. *Journal of*  
 433 *Geophysical Research*, 121(5), 854-870. <https://doi.org/10.1002/2016je005008>  
 434
- 435 Head III, J. W. (1974). Orientale multi-ringed basin interior and implications for the petrogenesis of lunar  
 436 highland samples. *The Moon*, 11, 327-356, 1974.  
 437
- 438 Head III, J. W. (1982). Lava flooding of ancient planetary crusts: Geometry, thickness, and volumes of  
 439 flooded lunar impact basins. *The Moon and the Planets*, 26, 61-88.  
 440
- 441 Head, J. W., & Lloyd, D. D. (1971). Near Terminator Photography. *Apollo 14 Preliminary Science Report*  
 442 *SP-272*, 297-300, NASA Special Publication.  
 443
- 444 Hiesinger, H., Head III, J. W., Wolf, U., Jaumann, R., & Neukum, G. (2002). Lunar mare basalt flow units:  
 445 Thicknesses determined from crater size-frequency distributions. *Geophysical Research Letters*, 29(8).  
 446 <https://doi.org/10.1029/2002GL014847>  
 447
- 448 Hiesinger, H., Head III, J. W., Wolf, U., Jaumann, R., & Neukum, G. (2011). Ages and stratigraphy of  
 449 lunar mare basalts: A synthesis. In W. A. Ambrose and D. A. Williams (Eds.), *Recent Advances and*  
 450 *Current Research Issues in Lunar Stratigraphy* (pp. 1-51). *Geological Society of America Special Paper*,  
 451 477. Boulder, CO: Geological Society of America. [https://doi.org/10.1130/2011.2477\(01\)](https://doi.org/10.1130/2011.2477(01))  
 452
- 453 Horz, F. (1978). How thick are lunar mare basalts? *Proceedings 9<sup>th</sup> Lunar and Planetary Science*  
 454 *Conference*, 3 (pp. 3311-3331). New York, NY: Pergamon Press, Inc.  
 455
- 456 Howard, K. A., Wilhelms, D. E., & Scott, D. H. (1974). Lunar basin formation and highland stratigraphy.  
 457 *Reviews of Geophysics and Space Physics*, 12, 309-327. <https://doi.org/10.1029/RG012i003p00309>  
 458
- 459 Johnson, B. C., Blair, D. M., Collins, G. S., Melosh, H. J., Freed, A. M., Taylor, G. J., et al. (2016).  
 460 Formation of the Orientale lunar multiring basin., *Science*, 354, 441-444.  
 461 <https://doi.org/10.1126/science.aag0518>  
 462
- 463 Lloyd, D., & Head, J. W. (1972). Orientale basin deposits (Riccioli area) in Apollo 16 earthshine  
 464 photography. In *Apollo 16 Preliminary Science Report, NASA Spec. Pap., SP-315* (pp. 29-24-29-26).  
 465 Washington, DC: National Aeronautics and Space Administration.  
 466
- 467 Needham, D. H., & Kring, D. A. (2017). Lunar volcanism produced a transient atmosphere around the  
 468 ancient Moon. *Earth and Planetary Science Letters*, 478, 175-178.

- 469 <https://doi.org/10.1016/j.epsl.2017.09.002>  
470  
471 Neumann, G. A., Zuber, M. T., Wieczorek, M. A., Head, J. W., Baker, D. M. H., Solomon, S. C., et al.  
472 (2015). Lunar impact basins revealed by Gravity Recovery and Interior Laboratory measurements. *Science*  
473 *Advances*, 1, 1-10. <https://doi.org/10.1126/sciadv.1500852>  
474  
475 Robinson, M. S., Ashley, J. W., Boyd, A. K., Wagner, R. V., Speyerer, E. J., Hawke, B. R., et al. (2012).  
476 Confirmation of sublunarean voids and thin layering in mare deposits. *Planet Space Sci*, 69(1), 18-27.  
477 <https://doi.org/10.1016/j.pss.2012.05.008>  
478  
479 Rutherford, M. J., Head III, J. W., Saal, A. E., Hauri, E. H., & Wilson, L. (2017). Model for the origin,  
480 ascent and eruption of lunar picritic magmas. *American Mineralogist*, 102, 2045-2053.  
481 <https://doi.org/10.2138/am-2017-5994>  
482  
483 Schaber, G. G. (1973). Lava flows in Mare Imbrium: Geologic evaluation from Apollo orbital  
484 photography. *Proceedings of the 4<sup>th</sup> Lunar Planetary Science Conference* (73-92).  
485  
486 Schulze-Makuch, D., & Crawford, I. A. (2018). Was there an early habitability window for Earth's Moon?,  
487 *Astrobiology*, 18(8), 985-988. <https://doi.org/10.1089/ast.2018.1844>  
488  
489 Smith, D. E., Zuber, M. T., Neumann, G. A., Lemoine, F. G., Mazarico, E., Torrence, M. H., et al. (2010).  
490 Initial observations from the Lunar Orbiter Laser Altimeter (LOLA). *Geophysical Research Letters*, 37,  
491 L18204. <https://doi.org/10.1029/2010GL043751>  
492  
493 Solomon, S. C., & Head III, J. W. (1979), Vertical movement in mare basins: Relation to mare  
494 emplacement, basin tectonics and lunar thermal history. *Journal of Geophysical Research*, 84(B4), 1667-  
495 1682.  
496  
497 Solomon, S. C., & Head III, J. W. (1980). Lunar mascon basins: Lava filling, tectonics and evolution of  
498 the lithosphere. *Reviews of Geophysics and Space Physics*, 18(1), 107-141.  
499  
500 Spudis, P. D. (1993). *The Geology of Multiring Impact Basins: The Moon and Other Planets*, Cambridge  
501 University Press: Cambridge, England.  
502  
503 Spudis, P. D., Wilhelms, D. E., & Robinson, M. S. (2011) The Sculptured Hills of the Taurus Highlands:  
504 implication for the relative age of Serenitatis, basin chronologies and the cratering history of the Moon.  
505 *Journal of Geophysical Research*, 116, E00H03, <https://doi.org/10.1029/2011JE003903>  
506  
507 Stöffler, D., Ryder, G., Ivanov, B. A., Artemieva, N. A., Cintala, M. J., & Grieve, R. A. F. (2006).  
508 Cratering history and lunar chronology. *Reviews in Mineralogy and Geochemistry*, 60, 519–596.  
509 <https://doi.org/10.2138/rmg.2006.60.05>  
510  
511 Thomson, B. J., Grosfils, E. B., Bussey, D. B. J., & Spudis, P. D. (2009). A new technique for estimating  
512 the thickness of mare basalts in Imbrium Basin. *Geophysical Research Letters*, 36(12), L12201,  
513 <https://doi.org/10.1029/2009gl037600>  
514  
515 Weider, S. Z., Crawford, I. A., & Joy, K. H. (2010). Individual lava flow thicknesses in Oceanus  
516 Procellarum and Mare Serenitatis determined from Clementine multispectral data. *Icarus*, 209(2), 323-336.  
517 <https://doi.org/10.1016/j.icarus.2010.05.010>  
518  
519 Whitten, J., Head III, J. W., Staid, M. I., Pieters, C. M., Mustard, J. F., Clark, R., et al. (2011). Lunar mare  
520 deposits associated with the Orientale impact basin: New insights into mineralogy, history, mode of  
521 emplacement, and relation to Orientale Basin evolution from Moon Mineralogy Mapper (M3) data from  
522 Chandrayaan-1. *Journal of Geophysical Research*, 116. <https://doi.org/10.1029/2010JE003736>  
523  
524 Whitten, J. L., & Head III, J. W. (2013). Detecting volcanic resurfacing of heavily cratered terrain:

- 525 Flooding simulations on the Moon using Lunar Orbiter Laser Altimeter (LOLA) data. *Planetary and Space*  
526 *Science*, 85, 24-37. <https://doi.org/10.1016/j.pss.2013.05.013>  
527
- 528 Williams, K. K., & Zuber, M. T. (1998). Measurement and analysis of lunar basin depths from Clementine  
529 altimetry. *Icarus*, 131(1), 107-122. <https://doi.org/10.1006/icar.1997.5856>  
530
- 531 Wilson, L., & Head III, J. W. (2018). Controls on lunar basaltic volcanic eruption structure and  
532 morphology: Gas release patterns in sequential eruption phases. *Geophysical Research Letters*, 45, 5852-  
533 5859. <https://doi.org/10.1029/2018GL078327>  
534
- 535 Yingst, R. A., & Head III, J. W. (1997). Volumes of lunar lava ponds in South Pole-Aitken and Orientale  
536 Basins: Implications for eruption conditions, transport mechanisms and magma source regions. *Journal of*  
537 *Geophysical Research*, 102(E5), 10,909-10,931.  
538
- 539 Zuber, M. T., Smith, D. E., Watkins, M. M., Asmar, S. W., Konopliv, A. S., Lemoine, F. G., et al. (2013).  
540 Gravity field of the Moon from the Gravity Recovery and Interior Laboratory (GRAIL) Mission. *Science*,  
541 339(6120), 668-671. <https://doi.org/10.1126/science.1231507>  
542
- 543 Zuber, M. T., Smith, D. E., Neumann, G. A., Goossens, S., Andrews-Hanna, J. C., Head, J. W., et al.  
544 (2016). Gravity field of the Orientale basin from the Gravity Recovery and Interior Laboratory Mission.  
545 *Science*, 354, 438-441. <https://doi.org/10.1126/science.aag0519>  
546  
547

548

549

**Figures:**

550

551

552 Figure S1. Volumes of erupted basalts and volatiles and lunar atmospheric pressure as a

553 function of time (from Needham and Kring, 2017). (a) Volume of erupted basalts as a

554 function of time, indicating peak volcanic activity primarily in Imbrium basin ca. 3.5 Ga;

555 the inset in each graph shows results for the time period from 3.0 Ga to 1.0 Ga at an

556 expanded scale. (b) Mass of volatiles, primarily CO and S, degassed during mare

557 emplacement. (c) Atmospheric surface pressure resulting from the volatiles released

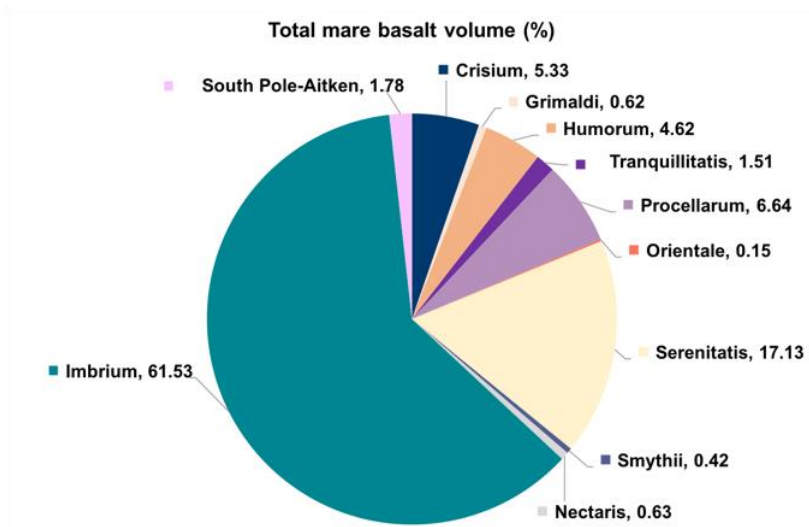
558 during mare emplacement, with a peak pressure  $\sim 1\%$  of Earth's current atmospheric

559 pressure, corresponding to peak volcanic activity 3.5 Ga. Quantified results for panel (a)

560 are included in Table S2, and for panels (b) and (c) in Table S3 of Needham and Kring

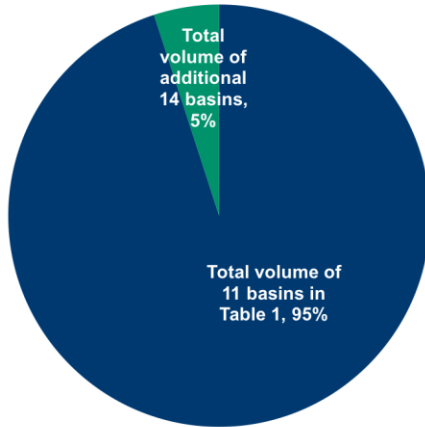
561 (2017).

561



562  
 563 a) Total mare basalt fill for the 11 basins considered in Table 1 of Needham and Kring  
 564 (2017).

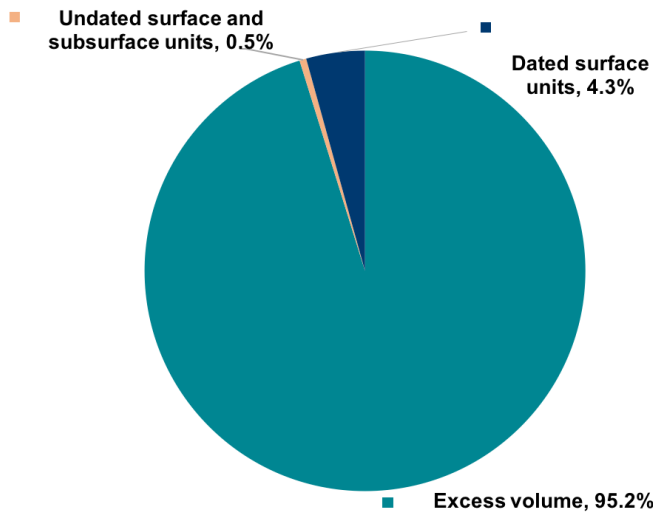
Percentage of total mare basalt volume in 11 major basins and 14 other basins used in the total mare basalt fill calculation of Needham and Kring (2017)



565  
 566 b) Percentage of total mare basalt volume in 11 major basins and 14 other basins used in.  
 567 the total mare basalt fill calculation of Needham and Kring (2017).  
 568



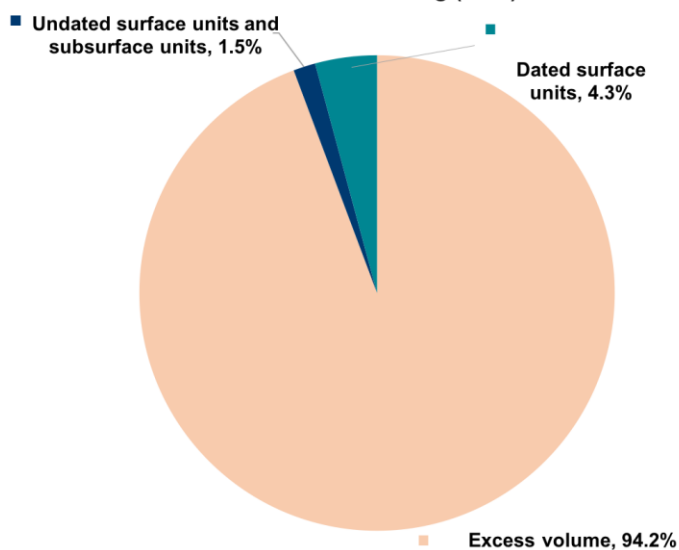
**Imbrium basin: Percentage of total mare fill in each of the categories (dated, undated, underlying, and excess) utilized by Needham and Kring (2017)**



569  
570  
571  
572

c) Imbrium basin: Percentage of total mare fill in each of the categories (dated, undated, underlying, and excess) utilized by Needham and Kring (2017).

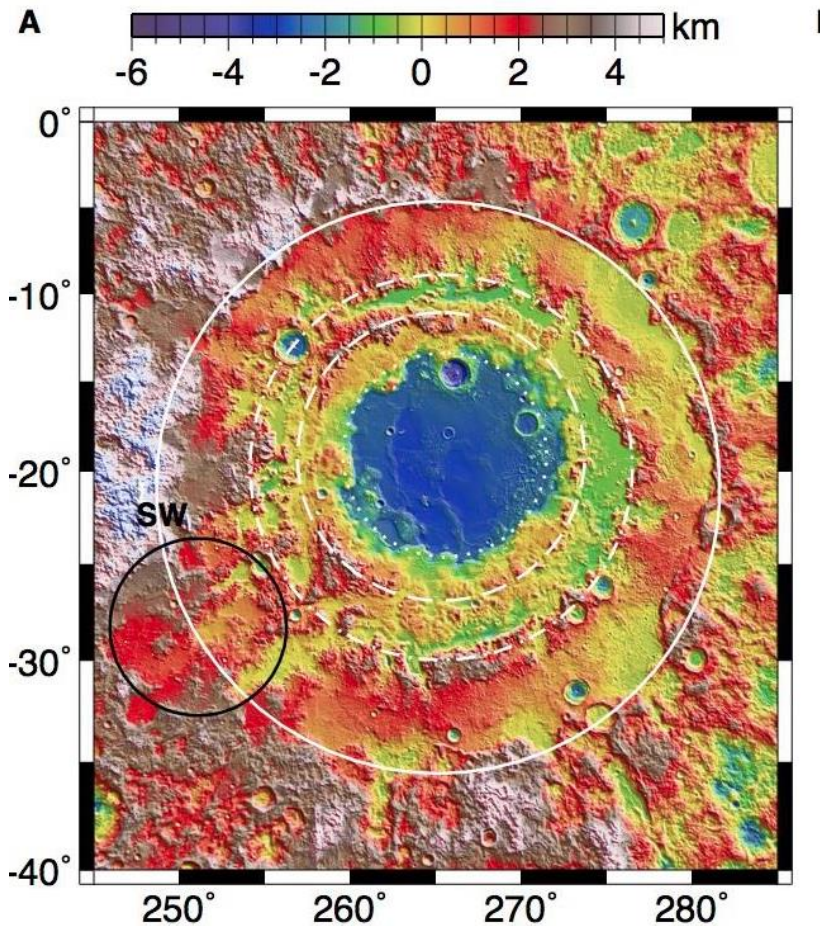
**Serenitatis Basin: Percentage of total mare fill in each of the categories (dated, undated, subsurface, and excess) utilized by Needham and Kring (2017)**



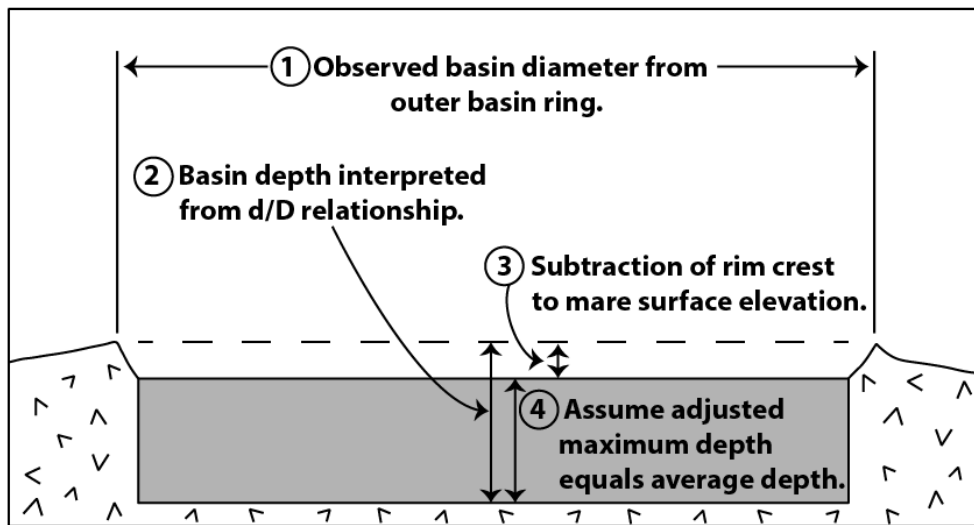
573  
574  
575  
576  
577  
578  
579

d) Serenitatis Basin: Percentage of total mare fill in each of the categories (dated, undated, underlying, and excess) utilized by Needham and Kring (2017). See Figure S3 for explanation of Needham and Kring (2017) unit age assignments.

Figure S2. Relative percentages of mare fill.



580



581

582 Figure S3. Topography of a typical multi-ring basin geometry and mare fill: a) Orientale

583 basin topographic map showing that the deepest part of the basin (blue) is not equivalent

584 to the average depth. b) Assumption that the maximum basin lava fill thickness is

585 equivalent to the average basin fill depth in the Needham and Kring (2017) model.

586

587

Needham and Kring Nomenclature	Candidate Sources of Uncertainty
<p>① Dated flow units (4.3%)</p> <p>② Undated and underlying flow units (0.5%)</p> <p>③ Excess flow volume (95.2%)</p> <p>Basin rim crest</p> <p>Cylindrical slab (assumes maximum depth equals average depth)</p>	<p>① Single dated flow unit may have multiple ages, durations.</p> <p>② Units assigned single age of oldest exposed dated flow unit: actual thicknesses, ages and durations unknown.</p> <p>③ "Excess" unit assigned single age of oldest dated flow: this unit certain to be multiple flow units of different ages, thicknesses, volumes and durations. - "Excess" volume overestimated due to assumption that maximum basin thickness = average thickness.</p>

588  
589  
590  
591  
592  
593  
594

Figure S4. Cross-section of a multi-ring basin lava fill illustrating assignments of different types of dated units by Needham and Kring (2017) and candidate sources of uncertainty in estimating basin lava fill thicknesses and volumes. Numbers in parentheses show the percentages of each type of unit assigned by Needham and Kring (2017) to age distributions in the Imbrium basin.